Frontiers in Satellite-Based Estimates of Cloud-Mediated Aerosol Forcing

Daniel Rosenfeld, Alexander Kokhanovsky, Tom Goren, Edward Gryspeerdt, Otto Hasekamp, Hailing Jia Jia, Anton Lopatin, Johannes Quaas, Zengxin Pan, Odran Sourdeval

Rosenfeld, D., Kokhanovsky, A., Goren, T., Gryspeerdt, E., Hasekamp, O., Jia, H., Lopatin, A., Quaas, J., Pan, Z., Sourdeval, O. (2023): Frontiers in Satellite-Based Estimates of Cloud-Mediated Aerosol Forcing. - Reviews of Geophysics, 61, 4, e2022RG000799.

https://doi.org/10.1029/2022RG000799

AGU ADVANCING EARTH AND SPACE SCIENCES

Reviews of Geophysics®

INVITED ARTICLE
10.1029/2022RG000799

Key Points:

- Calculating the susceptibility of clouds to aerosols has to include the cleanest conditions where measuring the aerosols is challenging
- The definition and use of regimes to group clouds with similar responses to aerosol is vital for future observation-based effective radiative forcing due to aerosol-cloud interaction (ERF_{aci}) estimates
- New observational tools are vital for reducing ERF_{aci} uncertainty but require further global climate model development to simulate these novel observables

Correspondence to:
D. Rosenfeld,
daniel.rosenfeld@huji.ac.il

Citation:
Rosenfeld, D., Kokhanovsky, A., Goren, T., Gryspeerdt, E., Hasekamp, O., Jia, H., et al. (2023). Frontiers in satellite-based estimates of cloud-mediated aerosol forcing. *Reviews of Geophysics*, *61*, e2022RG000799. https://doi.org/10.1029/2022RG000799

Received 3 APR 2023
Accepted 21 SEP 2023

Author Contributions:
Conceptualization: Alexander Kokhanovsky
Writing – original draft: Daniel Rosenfeld, Alexander Kokhanovsky, Tom Goren, Edward Gryspeerdt, Otto Hasekamp, Hailing Jia, Anton Lopatin, Johannes Quaas, Zengxin Pan, Odran Sourdeval

Frontiers in Satellite-Based Estimates of Cloud-Mediated Aerosol Forcing

Daniel Rosenfeld[1], Alexander Kokhanovsky[2], Tom Goren[3], Edward Gryspeerdt[4], Otto Hasekamp[5], Hailing Jia[6], Anton Lopatin[7], Johannes Quaas[6], Zengxin Pan[1], and Odran Sourdeval[7]

[1]Institute of Earth Science, The Hebrew University of Jerusalem, Jerusalem, Israel, [2]German Research Centre for Geosciences, Potsdam, Germany, [3]Department of Geography and Environment, Bar-Ilan University, Ramat Gan, Israel, [4]Grantham Institute—Climate Change and the Environment, Imperial College London, London, UK, [5]SRON Netherlands Institute for Space Research, Leiden, The Netherlands, [6]Institute for Meteorology, Leipzig University, Leipzig, Germany, [7]UMR 8518-LOA-Laboratory of Atmospheric Optics, CNRS, University of Lille, Lille, France

Abstract Atmospheric aerosols affect the Earth's climate in many ways, including acting as the seeds on which cloud droplets form. Since a large fraction of these particles is anthropogenic, the clouds' microphysical and radiative characteristics are influenced by human activity on a global scale leading to important climatic effects. The respective change in the energy budget at the top of the atmosphere is defined as the effective radiative forcing due to aerosol-cloud interaction (ERF_{aci}). It is estimated that the ERF_{aci} offsets presently nearly 1/4 of the greenhouse-induced warming, but the uncertainty is within a factor of two. A common method to calculate the ERF_{aci} is by the multiplication of the susceptibility of the cloud radiative effect to changes in aerosols by the anthropogenic change of the aerosol concentration. This has to be done by integrating it over all cloud regimes. Here we review the various methods of the ERF_{aci} estimation. Global measurements require satellites' global coverage. The challenge of quantifying aerosol amounts in cloudy atmospheres are met with the rapid development of novel methodologies reviewed here. The aerosol characteristics can be retrieved from space based on their optical properties, including polarization. The concentrations of the aerosols that serve as cloud drop condensation nuclei can be also estimated from their impact on the satellite-retrieved cloud drop number concentrations. These observations are critical for reducing the uncertainty in the ERF_{aci} calculated from global climate models (GCMs), but further development is required to allow GCMs to properly simulate and benefit these novel observables.

Plain Language Summary Aerosols affect the climate in many ways, including serving as the basis for the formation of cloud droplets. Therefore, aerosols have profound impacts on clouds and through that on the Earth's energy budget. Increasing aerosols leads to additional cloud droplets, changing cloud properties such that they reflect more solar radiation back to space and offset nearly 1/4 of the warming induced by greenhouse gases, but with a large uncertainty within a factor of two. Here we review the ways by which aerosols and their radiative effects are retrieved from space. A major challenge is to reduce the uncertainty by better retrieval methods of atmospheric aerosol and cloud properties. This challenge is met by rapid satellite retrieval methodological developments and numerous new satellite missions, which are described here. These new methodologies have to be matched with parallel development in the global circulation models for the improved estimation of the actual climatic impacts.

1. Introduction

Atmospheric air contains various liquid and solid particles (usually with sizes in the range of 0.1–10 μm although smaller and larger particles occur as well), in addition to hydrometeors (cloud and precipitation particles). These particles (known as aerosols) are lifted from the surface of the planet due to wind, produced by anthropogenic emission, or originate directly in the atmosphere from the gas phase. Importantly, aerosol particles can serve as nuclei for water droplets and ice crystals that form the clouds in our atmosphere. Without these nuclei, clouds, precipitation (see Figure 1), and life on the planet would be very different. In addition, clouds increase the planetary albedo to the level at which life as we know is possible.

Anthropogenic aerosols are responsible for reflecting solar radiation both directly and through their interactions with clouds. These effects could offset more than a quarter of the warming that is induced by anthropogenic green-

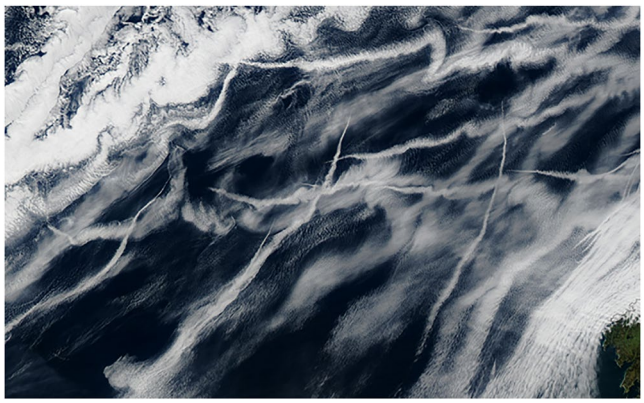

Figure 1. Ship track clouds in the East Atlantic to the northwest of Spain. The air is so clean that cloud droplets cannot form except on the aerosol plumes emitted from ship stacks, which form the ship track clouds. The scene width is 500 km. Taken from Moderate Resolution Imaging Spectrometer Aqua on 8 March 2008.

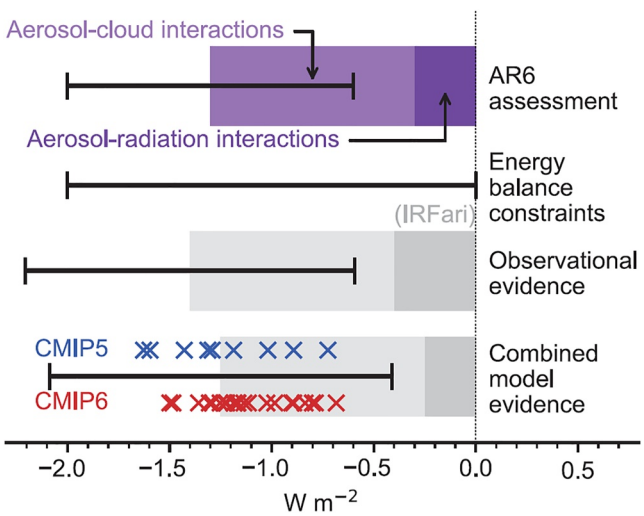

Figure 2. Aerosol direct and cloud-mediated radiative forcing. After Figure 7.5 of the IPCC sixth assessment report of WG-I. The upper bar shows the assessment, based on the combination of the global energy balance constraints that require the aerosol effect to be within these bounds (second bar); The observational estimates (third bar); and the model estimates (fourth bar).

house gases (Forster et al., 2021). However, the uncertainty in this estimate is a factor of two (Bellouin et al., 2020; IPCC-AR6). Only about a quarter of the cooling by the anthropogenic aerosol radiative forcing occurs by direct absorption and reflection of the solar radiation by the aerosol particles. The remaining nearly 3/4 of the aerosol radiative forcing is mediated by clouds (Figure 2).

By playing an important role in the formation of clouds, aerosols affect cloud macrophysical, micro-physical, and radiative properties in multiple ways, which include, for example:

(a) *The albedo effect*: Aerosols serve as cloud drop condensation nuclei (CCN). Clouds that form in the air with added aerosols have more numerous droplets. Even if these droplets are smaller, they collectively have a larger surface area for the same amount of liquid water path (LWP). Since light is scattered from the droplet surface, the cloud optical thickness (COT) and cloud albedo increase with added CCN and cloud droplet number concentrations (N_d) (Twomey, 1974, 1977). This effect is also known as the radiative forcing due to aerosol-cloud interaction, RFaci (Boucher et al., 2013; Forster et al., 2021). A secondary impact on the albedo is incurred by the dispersion effect (ν). Widening the dispersion of the drop size distribution reduces the cloud albedo (Peng & Lohmann, 2003).

(b) *The LWP effect*: As N_d is perturbed, other cloud quantities may rapidly adjust (also known as adjustments to aerosol-cloud interactions (ACI)). One of these effects is the changes in the cloud LWP, which generally increases with the square of the cloud's vertical extent. Droplet coalescence is approximately proportional to the fifth power of cloud drop effective radius (r_e) (Freud & Rosenfeld, 2012). Adding CCN to raining clouds reduces r_e, coalescence and hence reduces the loss rate of cloud water by rainfall, thus increasing LWP (Albrecht, 1989). However, the smaller resulting cloud drops evaporate faster upon mixing with ambient air, thus decreasing LWP, mainly for non-precipitating clouds (Ackerman et al., 2004; T. C. Chen et al., 2011). As droplet sedimentation rates are reduced, cloud-top liquid water content (LWC) is increased. This enhances cloud-top radiative cooling, leading to increases in cloud-top entrainment and decreases in LWP, depending on relative humidity above cloud tops (Ackerman et al., 2004; Bretherton et al., 2007). The enhanced evaporation with increased N_d starts dominating when N_d exceeds ~30 cm^{-3} (Gryspeerdt et al., 2019).

(c) *The cloud depth effect*: The CCN can enhance clouds with small N_d also by increasing the condensation efficiency when a more integrated drop surface area is available for condensation and respective latent heating (J. Fan et al., 2018; Koren et al., 2004). This may be a reason for LWP increasing with N_d for N_d < 30 cm^{-3}, as seen in satellite statistics (e.g., Gryspeerdt et al., 2019). Large uncertainties in such quantifications remain (e.g., Arola et al., 2022).

(d) *The cloud cover effect*: Cloud horizontal extent also adjusts to N_d perturbations. Rain produces downdrafts that lead eventually to cloud dissipation and the triggering of new clouds (Rosenfeld et al., 2006). Adding CCN can reduce rainfall from raining clouds, enhancing their longevity and areal coverage (Albrecht, 1989).

(e) *The cloud-burning effect*: Radiation-absorbing aerosols can heat the clouds and partially or fully evaporate them, thus inducing a positive radiative forcing, that is, a warming effect (Ackerman et al., 2000).

(f) *The cloud pollution effect*: Clouds are highly reflective in the visible spectrum. Aerosols containing soot and dust can lower cloud reflectance in the visible, leading to a positive aerosol forcing.

(g) *The cloud position effect*: Depending on the position of the aerosol layer (above, inside, or underneath the cloud field, including broken cloud fields), various cloud-mediated aerosol forcing effects occur. For example, absorbing aerosols above clouds can enhance the cloud cover due to less solar heating, whereas aerosols coinciding with the clouds can lead to decreased cloud cover due to the cloud-burning effect (Z. Lu et al., 2018; Wilcox, 2010).

Effect (f) is a part of the radiative forcing due to aerosol-radiation interactions (also known as "direct effect"). Effects (e) and (g) are adjustments to aerosol-radiation interactions (Boucher et al., 2013). These elements of ACI are not the focus of this review. We focus mainly on the ways by which CCN affect clouds, thus mainly on the cloud albedo and cover effects which have a comparable impact, and on the LWP effect. Together, these microphysically triggered effects comprise the majority of the ERF_{aci} (Bellouin et al., 2020).

Some of the effects listed above are highly dependent on the underlying surface type (ocean, desert, snow, ice, vegetation), which complicates the analysis even further. Most studies have focused on the better-understood marine low cloud, partly due to difficulties in retrieving cloud and aerosol properties over varying surfaces (see Section 3). Aerosols effects on deep convective clouds are further complicated by the existence of the ice phase and its direct sensitivity to ice-nucleating particles (Cantrell & Heymsfield, 2005), and indirect sensitivity to CCN effects on the liquid water part of the clouds (J. Fan et al., 2013).

The albedo effect is nearly instantaneous. The LWP and cloud cover effects occur in response to the change in condensation, evaporation, and precipitation rates of the clouds, thus having a delayed response on the scale of the cloud lifetime. Longer-term effects occur through cloud-mediated impacts on the thermodynamic structure of the boundary layer (a process that can take several hours), which feed back to the clouds' dynamical, microphysical, and radiative properties when they adjust to these modified conditions (Dagan et al., 2018). The effective radiative forcing of ACI (ERF_{aci}) includes both nearly instantaneous RFaci and rapid cloud adjustments to aerosol perturbation. Much slower additional changes can occur as sea surface temperature and other climate elements adjust to the changes in cloud properties, which may feedback to the cloud properties.

A critically important metric of the aerosol effects on clouds is the susceptibility, which is defined as a fractional change of a cloud property for the fractional change in aerosol amount (Bellouin et al., 2020; Feingold, 2003). In-situ and surface-based measurements of ACI are too sparse and plagued with large meteorological variability. A very large amount of measurements need to be collected at a global scale to ensure coverage of the various regimes and reduce the impacts of meteorological variability. Therefore, the susceptibility of various cloud properties to aerosols at regional and global scales can be measured only with satellites, which can provide both aerosol and cloud properties globally, albeit in general not simultaneously. Satellite retrieval algorithms can be used to estimate the cloud radiative effect (CRE), which is the difference between the top of the atmosphere net radiation with and without the cloud. The change of CRE with aerosols is defined as the susceptibility of CRE to aerosols multiplied by the fractional change in aerosols. The susceptibility is considered to be a forcing only when the change in aerosols is forced externally to the natural Earth radiative balance, such as anthropogenic or volcanic emissions.

The anthropogenic contribution to the total aerosols cannot be readily observed and must be calculated by models based on estimated emission sources. Therefore, global climate models (GCMs) are required for calculating ERF_{aci}. In principle, the ERF_{aci} is calculated by the multiplication of the CRE by the product of the susceptibility N_d and the fractional change in N_d due to anthropogenic emissions (Bellouin et al., 2020; Hasekamp et al., 2019b). The satellite retrievals of cloud and aerosol properties have large uncertainties, which are carried into the satellite-calculated susceptibilities. The satellite-retrieved aerosol effective radiative forcing and its large uncertainty are shown in the third bar of Figure 2. The uncertainties of the satellite observations of ERF_{aci} will be dealt with in-depth in this review.

Climate models can calculate directly the ERF_{aci} as well as the susceptibility from their internal representation of ACI. However, the physical representation of clouds in general and ACI, in particular, is crude, partly due to limitations in resolution and computation power, and partly due to a lack of understanding or overly coarse parameterization of the respective mechanisms. Even in new-generation kilometer-resolution climate models, ACI needs to be parameterized (Stevens et al., 2020a, 2020b). Furthermore, the assumptions on ACI for deep convective clouds are presently very crude and often absent in GCMs, although the available parameterizations have shown improved realism of the simulations (Gettelman et al., 2015; Lohmann, 2008; Song & Zhang, 2011).

The aerosol-effective radiative forcing as calculated by GCMs is shown in the fourth bar of Figure 2 and is similar in magnitude and uncertainty to the satellite-based forcing. This similarity is not entirely independent due to the role of satellite observations in developing and tuning GCM parameterizations (Stevens et al., 2016) and the role of GCMs in determining the anthropogenic aerosol fraction for the satellite-based estimates. Therefore, satellite retrievals of the susceptibility are essential for the calculations of ERF_{ACI} by tuning the parameterization of the susceptibility of the GCMs (Quaas et al., 2006). Remarkably, the uncertainty of both observational and combined model lines of evidence still exceeds the energy balance constraints (Bellouin et al., 2020). It demonstrates that the satellite-observation-based bottom-up estimates are still too uncertain to significantly reduce the uncertainty in ERF. The uncertainty in the aerosols ERF propagates to the uncertainty in climate sensitivity (Watson-Parris and Smith, 2022). A larger aerosol forcing offsets respectively more greenhouse gas forcing that led to the global warming that has occurred so far, to which the GCMs are constrained to reproduce (Anderson et al., 2003a, 2003b).

It is today a prevailing view that most of the aerosol forcing is related to liquid-water clouds rather than to ice and mixed-phase clouds, although the impact of the two latter remains largely uncertain (Bellouin et al., 2020). The net radiative perturbation due to cirrus has indeed been reported as being very small in GCMs (Penner et al., 2018; Zhu and Penner, 2020) but such estimates have not yet been confirmed from observations and do not include the wide variety and complexity of ice nucleation mechanisms responsible for adjustments. Satellites rarely provide adequate cloud properties to quantify the above-mentioned effects, such as the number concentration of ice crystals (N_i), even if recent progress was made in this direction (Sourdeval et al., 2018) and ACI effects have now been quantified regionally and globally from observations (e.g., Gryspeerdt et al., 2018; B. Zhao et al., 2018). Mixed-phase clouds are still very poorly constrained from satellite observations, as there exist almost no reliable products providing their microphysical properties. Their role in ACI studies can still be important to determine as they can originate from liquid-water clouds (Coopman et al., 2018). Finally, the aerosols that serve as ice nuclei are also difficult to quantify (Hoose & Möhler, 2012) and their transport to high altitudes in GCMs or reanalysis products is more uncertain, making the susceptibility challenging to estimate for ice and mixed-phase clouds. Because of such high uncertainties and the early stage of satellite aerosol forcing studies for ice and mixed-phase clouds, this review will largely focus on liquid clouds. However, it can be kept in mind that some demonstrations and conclusions taken here can apply to ice and mixed-phase clouds (e.g., by replacing N_d with N_i which is the number of ice particles, in Section 2).

This article reviews the causes of the observational uncertainties, which are dominated by uncertainties of satellite observations. Despite these uncertainties, there are no other viable methods for global observations. The principles of calculating ERF_{aci} are described in Section 2. The required measured quantities are given in Section 3, and issues and biases with their measurements are described in Sections 4 and 5. Clouds and aerosol adjustments and feedback to initial changes in the aerosols are described in Section 6. Finally, a summary, outlook, and recommendations are given in Section 7.

2. The Radiative Forcing

2.1. The Radiative Forcing Equation

The effective radiative forcing due to ACI, ERF_{aci}, is the perturbation of the top-of-atmosphere net radiation budget, R, attributable to the anthropogenic perturbation of clouds due to ACI (Boucher et al., 2013; Forster et al., 2021) at fixed SST. The relevant bulk properties of liquid-water clouds that determine their radiative effect are their horizontal extent, expressed as the fractional horizontal coverage of a scene by clouds, the cloud fraction f; cloud vertically-integrated LWC or LWP, related to the cloud vertical thickness; cloud droplet number concentration, N_d; and the cloud droplet size spectrum dispersion, ν (Quaas & Gryspeerdt, 2022). The cloud-top temperature T_{top} is also relevant for the cloud greenhouse effect, but for liquid-water clouds the greenhouse effect is small, offsetting only about 10% of the short-wave radiative effect, so this aspect is neglected here.

Thus, R in our assessment is the solar top-of-atmosphere net flux. This solar flux in a scene may be split into the contribution of clouds, R_{cld}, that is relevant in the cloud-covered fraction of the scene, and the contribution by the clear-sky fraction of the scene, R_{clr}: $R = fR_{cld} + (1 - f)R_{clr}$. It may also be written in terms of the CRE, $C = R - R_{clr}$ as $R = C + R_{clr}$. The foremost anthropogenic perturbation of clouds due to ACI is the anthropogenic perturbation of cloud droplet number concentration (Bellouin et al., 2020; Rosenfeld et al., 2019), $N_{d,ant}$, taken

here as a vertically-constant field. This can be derived from the sensitivity of N_d to cloud-active aerosol, α, and the anthropogenic perturbation of the aerosol properties, $\Delta\alpha_{ant}$:

$$\Delta \ln N_{d,ant} = \frac{\partial \ln N_d}{\partial \ln \alpha} \Delta \ln \alpha_{ant} \quad (1)$$

The aerosol metric α is ambiguous here. The most direct option for α is the cloud condensation nuclei number at the cloud base but other choices are possible, such as the aerosol optical depth (AOD) and aerosol index (AI), which are related to the CCN (Feingold et al., 2003; McComiskey et al., 2009). The susceptibility term $\partial \ln N_d / \partial \ln \alpha$, is strongly state-dependent (e.g., Jia et al., 2022).

The most fundamental perturbation of the Earth's radiation budget is thus the radiative forcing due to ACI given in Equation 2:

$$RF_{aci} = \frac{\partial R}{\partial \ln N_d} \Delta \ln N_{d,ant} \quad (2)$$

where the relative perturbation in droplet number, $\Delta \ln N_{d,ant}$, is considered due to the impact of N_d on radiation is approximated as a logarithmic function (e.g., Bellouin et al., 2020; Carslaw et al., 2013). This definition of RF_{aci} still neglects that the sensitivity and droplet number perturbation are regime-dependent. However, the other three quantities (drop dispersion, cloud fraction, and LWP) also alter R and are themselves altered once an anthropogenic perturbation of cloud droplet number took place, leading to three more terms that contribute to the RF_{aci}, which, according to Equation 3, becomes the effective RF_{aci}, or ERF_{aci}.

$$ERF_{aci} = \sum_{regime} \left(\omega_{reg} \left[\frac{\overline{\partial R}}{\partial \ln N_d}|_{LWP,f} + \frac{\overline{\partial R}}{\partial \nu} \frac{\overline{\partial \nu}}{\partial \ln N_d} + \frac{\overline{\partial R}}{\partial f} \frac{\overline{\partial f}}{\partial \ln N_d} + \frac{\overline{\partial R}}{\partial LWP} \frac{\overline{\partial LWP}}{\partial \ln N_d} \right] \overline{\Delta \ln N_{d,ant}} \right) \quad (3)$$

As clear-sky radiation is unaffected by ACI, R in Equation 3 may be replaced by the CRE. The terms of Equation 3 are: The albedo effect for a given LWP and cloud fraction (the Twomey effect) is $\overline{\partial R}/\partial \ln N_d|_{LWP,f}$; The cloud drop dispersion (ν) effect on CRE is $\overline{\partial R}/\partial \nu \overline{\partial \nu}/\partial \ln N_d$; The cloud fraction effect on CRE is $\overline{\partial R}/\partial f \overline{\partial f}/\partial \ln N_d$; And the LWP effect on CRE is $\overline{\partial R}/\partial LWP \overline{\partial LWP}/\partial \ln N_d$. The sensitivity for constant LWP and f, multiplied by the change in N_d and integrated over regimes, indeed, is the global RFaci. The LWP and N_d are obtained from cloud drop effective radius (r_e) and optical depth by Equations 4 and 5, respectively. The sum of these terms in the square brackets in Equation 3 is the total dependence of CRE on N_d in, say, a 1 × 1 degree scene that contains clouds, expressed as dCRE/$d\ln N_d$. The causal relationships between LWP and aerosols are discussed in Section 6.2.

A key point we stress in this review is the consideration that clouds can be categorized into different types (Howard, 1803; WMO, 1975, 2017). Different cloud types such as cumulus, stratus, or stratocumulus originate from different weather phenomena and in particular have different turbulent updraft characteristics. For these reasons, different cloud types, or cloud regimes, respond differently to aerosol perturbations (Stevens and Feingold, 2009). Examples of regime classification are given in Figures 3 and 4 and further discussed in Section 2. Thanks to a definition of cloud regimes that behave similarly enough to ACI, then, we do not need to assess sensitivities in their full spatiotemporal variability but only need to consider these regimes. The ERF_{aci} in the global mean can then be expressed in Equation 3 as the sum over all cloud regimes, weighted by their frequency of occurrence, ω_{reg}. Equation 3 is central to this review, by formulating the way to obtain the ERF_{aci} from the relevant observed cloud and aerosol properties and the change in these aerosol properties from pre-industrial to present-day levels. This then sets the stage for the rest of the review and the way that we attempt to build knowledge of each element of the equation.

2.2. Summation Over Regimes

ACI depend on the regime (Stevens and Feingold, 2009), necessitating the consideration of regimes in the ERF calculation. Previous studies have implicitly attempted to account for regimes by using regional variation of the terms in Equation 3 (e.g., Quaas et al., 2008). However, cloud regime spatial variations across these regions can generate confounding relationships (Grandey & Stier, 2010), an occurrence of Simpson's Paradox. Following this, most recent work has calculated the susceptibilities in Equation 3 at 1 × 1° spatial resolution (such as Bellouin

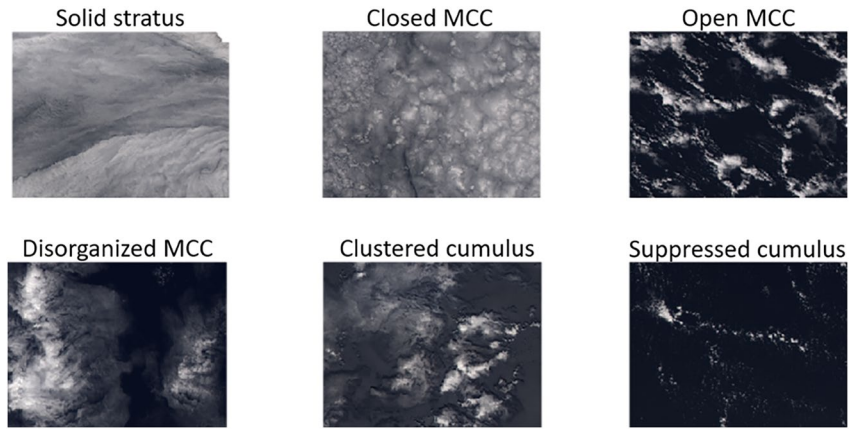

Figure 3. Cloud classification of marine boundary layer clouds by their appearance. The scenes are Moderate Resolution Imaging Spectrometer images of nearly 128 × 128 1-km pixels. The classification was done objectively by supervised machine learning. From Mohrmann et al. (2021).

et al., 2020, where this spatial variation is encoded in the "effective cloud fraction"). Although this addresses the confounding impact of cloud regimes spatial variability, the impact of temporal variability remains; the variation is even required when calculating susceptibilities in all but a few special cases; for example, Toll et al., 2017).

By selecting "similar" clouds when calculating the susceptibilities in Equation 3, a summation by regimes allows data to be aggregated over a much larger area. However, the method for selecting regimes that contain these "similar" clouds is not straightforward. There are two main methods for defining regimes used in the literature:

Cloud regimes are defined based on observed cloud properties, including cloud fraction, cloud top pressure and optical depth (Oreopoulos et al., 2014; Rossow et al., 2005), updraft and precipitation state (Jia et al., 2022), and cloud geometrical thickness (Rosenfeld et al., 2019). Recent work has also proposed using cloud organization, based on machine-learned (Figure 3; Mohrmann et al., 2021) or human-specified regimes (Stevens et al., 2020a, 2020b) definitions. These regime definitions often overlap. For example, the gravel and fish of Stevens et al. (2020a, 2020b) approximately match the clustered cumulus and the open marine cellular convection (MCC) is Mohrmann et al. (2021). By relying on observed properties of the clouds, cloud regimes provide a powerful method for representing the state of the atmosphere. However, these cloud properties may also change in response to aerosol, which can result in potentially undesirable aerosol-induced changes to cloud regime occurrence. For example, the changes in cloud cover, cloud fraction, and precipitation between the regimes of closed and open MCC are driven by aerosols (Rosenfeld et al., 2006). Furthermore, by definition, the $\overline{\partial f}/\partial \ln N_d$ vanishes to zero in closed MCC.

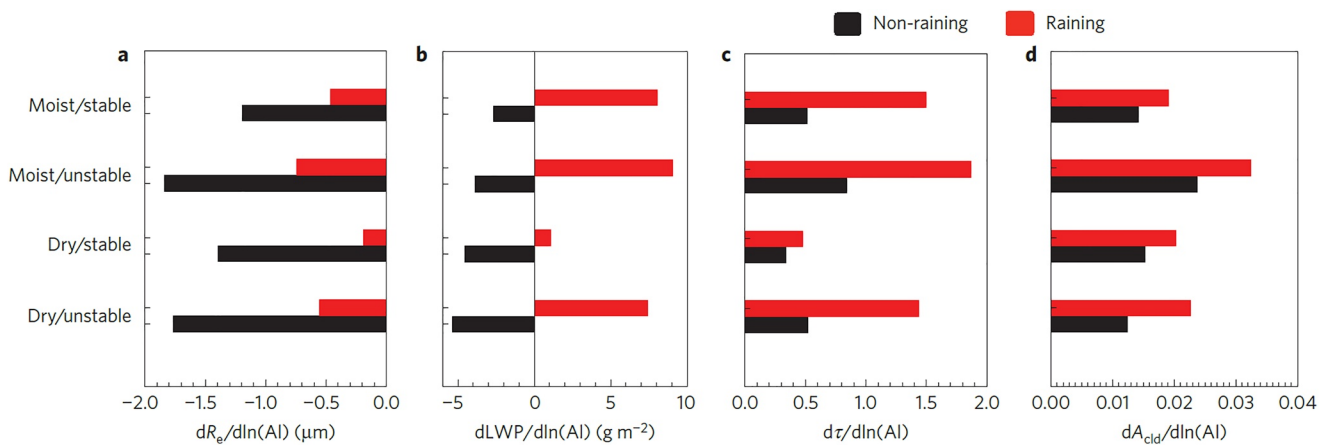

Figure 4. The dependence of cloud properties to aerosol index (AI, the product of aerosol optical depth and Angström exponent, which is a proxy to CCN) on low tropospheric stability, free tropospheric relative humidity (RHft), and non-raining/raining conditions. The panels show the susceptibility to AI of (a) cloud drop effective radius; (b) cloud liquid water path; (c) cloud optical depth; and (d) cloud albedo. From Y.-C. Chen et al. (2014).

In contrast, *meteorological regimes* are defined by the cloud-controlling factors, rather than the observed clouds. All clouds develop following the same physical laws, such that if the environment can be adequately specified, the resulting cloud can be determined; this is the principle behind cloud parametrizations. These regimes are defined using factors independent of aerosol concentration, such as vertical wind (Koren et al., 2005), low troposphere stability (Y.-C. Chen et al., 2014), convective state (Dipu et al., 2022), and aerosol type (L'Ecuyer et al., 2009). Being defined separately from aerosol concentrations and cloud properties that might change in response to these aerosols is an advantage when investigating ACI, although it requires accurate measurements of the cloud-controlling factors.

Not all regime definitions fall into one of these types alone. Some regime definitions include criteria from both categories, such as low troposphere stability and precipitation state (Y.-C. Chen et al., 2014; Figure 4).

Given the wide range of potential variables to use for separating regimes, it is not clear that there is a single "best" regime definition. However, when investigating ACI, regime decompositions are broadly aiming to achieve two key purposes:

(a) *Accounting for sampling biases* (cf. Section 4.2). Retrievals are not performed in all locations, with some regimes being more poorly sampled. If this biased sampling is not accounted for, the regimes will be under-represented in the global statistics, resulting in a biased ERF_{aci} estimate. For example, $\partial \ln N_d / \partial \ln \tau_a$ (where τ_a is AOD), is often observed to be stronger in stratocumulus clouds compared to shallow cumulus (Gryspeerdt & Stier, 2012; Jia et al., 2021). If these regime-based differences are not accounted for, sampling differences in the regimes (due to a differing cloud fraction e.g.,) can bias the ERF_{aci} calculation (Jia et al., 2021).

(b) *Reducing spurious correlations*. When data from different cloud regimes are combined, the resulting correlations can have different magnitudes or signs, biasing ERF_{aci} estimates. For example, N_d responds differently to aerosol in precipitating and non-precipitating clouds. N_d is on average different in these two precipitation regimes. When calculating $d \ln N_d / d \ln \tau_a$ for all the data together, the covariation in N_d and τ_a caused by precipitation produces a confounded estimate of the susceptibility (Jia et al., 2022).

It is important to note that different regime definitions may be required to investigate different processes, indeed Equations 1 and 3 require different regime definitions. This limits the usefulness of a direct comparison between regimes to specific cases. However, given the purposes of a regime decomposition, some key properties of any regime definition can be described. These properties also describe tests that the regime definition should satisfy. The regimes should:

2.2.1. Produce No Change in Occurrence as Aerosols Are Changed

For a given regime definition, as aerosols are changed, the properties and occurrence of the regimes might change. For example, cloud regimes (Jakob & Tselioudis, 2003; Jin et al., 2017) are defined using cloud fraction, cloud optical depth, and cloud top pressure. However, cloud regime definitions that depend on aerosols are unsuitable for quantifying aerosol effects. If cloud fraction increased with increasing aerosol (as is expected), this would produce both an increased occurrence of the high cloud fraction regimes (e.g., Gryspeerdt et al., 2014) and a change in the average cloud fraction of the regimes (due to a changing cloud fraction distribution). Calculating the ERF_{aci} then requires not only an analysis of how the regimes have changed but an analysis of the change in the occurrence of the regime (and potentially the combination of these two effects). This complicates the calculation of the ERF_{aci} using present-day data and requires a GCM to estimate changes in regime frequency (Langton et al., 2021).

The regime decomposition thus needs to be defined such that the regime definition is independent of properties that would be impacted by aerosol variations (such as cloud fraction) although this is difficult. While updraft and aerosol-limited conditions are often considered when looking at ACI, they are not suitable to be used as cloud regimes for this analysis under this requirement. As aerosol concentrations increase, it would be expected to move toward an updraft-limited condition, such that these conditions have a different occurrence in the pre-industrial atmosphere. Similarly, while ISCCP cloud regimes have been used for the analysis of ACI (Gryspeerdt & Stier, 2012), they are not suitable under this requirement, as COT, top pressure and fraction (used in the regime definition) vary with aerosol concentration (Albrecht, 1989; Gryspeerdt et al., 2016; Kaufman et al., 2005). The use of meteorological parameters (e.g., low tropospheric stability (LTS) and vertical motion at 500 hPa (ω500); Medeiros & Stevens, 2011) is one method to define regimes that do not vary significantly with

aerosol. Assuming that the aerosol impact on these properties is minimal, this regime occurrence is independent of aerosol. However, this regime classification may not be sufficient to characterize the cloud field (Nam & Quaas, 2013), leading to the second requirement.

2.2.2. Be Specific Enough to Avoid Simpson's Paradox

Simpson's paradox occurs due to a poor selection of controlling variables, leading to an erroneous attribution of causality. For example, large-scale variation in AOD and N_d fields in addition to the causal impact of aerosols on N_d can lead to difficulties in characterizing the causal relationship (Grandey & Stier, 2010).

An ideal regime decomposition here should not change in properties as it is further decomposed. If new regimes are created that satisfy criterion 1, these sub-regimes should still have the same properties (e.g., susceptibility) as the original larger regime. This suggests that regimes should not have geographic variation—as clouds are expected to behave the same independent of geographic location, the occurrence of geographic variation in the regime properties indicates that the regime definition may not be specific enough.

However, care should be taken when using linear relationships to characterize inherently non-linear processes. This can create the appearance of geographical variation (and hence Simpson's paradox), by sampling different sections of the same non-linear relationship in different geographic regions (e.g., polluted and clean locations).

2.2.3. Have Enough Data to Reach Statistical Significance

While criterion (b) above sets an upper limit to the population of a cloud regime, the regimes should not be sliced indefinitely, such that each regime contains only a small number of data points. This then creates significant uncertainty around the statistics for the regime properties. The exact lower limit of the regime population is determined by the requirements of the particular study. It is naturally important that the regime populations are large enough that statistics calculated for them are statistically significant.

Circulation properties, coupling state, advection rates, synoptic forcing, and surface properties are all examples of potential regime definitions that may satisfy the above criteria, depending on the requirements of an individual study. If the observational study is to be used for comparison to models, care should be taken to select regimes that can be identified in the model output.

3. Measurements of the Required Quantities

Following Equation 3, cloud observations of N_d, ν, f, r_e, LWP, and R or CRE are needed to quantify ERF_{aci}. Here, the derivation of N_d, ν, and LWP, requires an underlying knowledge of the cloud Particle Size Distribution (PSD) and the Cloud Optical Depth (τ_c). Furthermore, a key step in the quantification of ERF_{aci} is the derivation of the anthropogenic perturbation of N_d, which requires the retrieval of the amount of cloud active aerosol and the retrieval or simulation of its anthropogenic perturbation. This requires the retrieval of aerosol concentration size distribution and vertical distribution. This can be partially addressed by retrieving the AOD (or τ_a) and Angström Exponent (AE) and/or related optical properties such as the refractive index. An alternative method is retrieving the CCN activity of the aerosols from retrieved N_d and cloud base supersaturation, S_b, as obtained from N_d and the retrieved cloud base updraft, W_b.

3.1. Cloud Properties

Terrestrial clouds are composed of water droplets and/or ice crystals. The cloud albedo and optical depth are determined by their N_d, r_e, LWP (or their equivalents for ice clouds) and the dispersion of the drop size distribution, ν. The r_e and ν determine the cloud PSD.

The cloud drop effective radius is defined as $r_e = \int r^3 n(r) dr / \int r^2 n(r) dr$, that is, the third divided by the second moment of the cloud drop size distribution $n(r)$. The r_e depends on the PSD with r_e relationship of $k = (r_v/r_e)^3$, where r_v is the mean volume radius, that is, the drop radius if all drops had an equal radius for the given cloud water content. Typically, $r_e = 1.08 r_v$ (Freud & Rosenfeld, 2012), which implies $k = 0.8$.

The r_e can be retrieved together with the τ_c from radiometric bi-spectral satellite measurements in the visible and shortwave infrared (Nakajima & King, 1990). Here, the reflectance in the visible part of the spectrum is sensitive to τ_c but not much to r_e. The reflectance in a shortwave infrared spectral band where absorption of radiation by

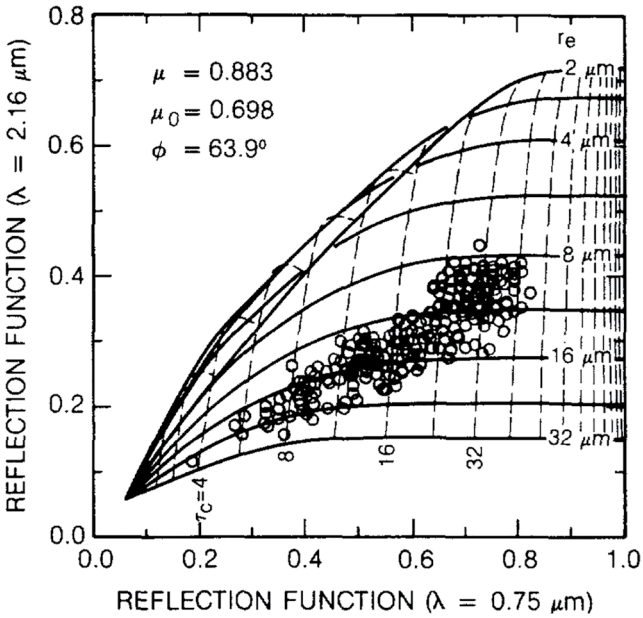

Figure 5. Theoretical relationships between the cloud drop effective radius and the reflection function at the wavelengths 0.75 and 2.16 microns for various values of cloud optical thickness (calculated at the wavelength $\lambda = 0.75$ μm). Data from measurements above marine stratocumulus clouds during FIRE on 10 July 1987 are superimposed on the figure. From Nakajima and King (1990).

water droplets becomes substantial (e.g., typically, wave bands of 1.6, 2.1, and 3.7 microns are used), is sensitive to both r_e and τ_c. So, the combination of a spectral band in the visible and one in the shortwave infrared can provide both r_e and τ_c. Such retrievals can make use of tabulated values of reflectance or approximations for radiative transfer (Kokhanovsky, 2006), and shown as a diagram in Figure 5.

The values of τ_c and r_e can be used to determine LWP, as:

$$\mathrm{LWP} = k\rho_w r_e \tau_c \tag{4}$$

where ρ_w is liquid water density and $\kappa = 0.8$ is assumed. $k = 2/3$ can be used when cloud properties are considered vertically constant, or $k = 5/9$ when following an adiabatic growth model for the cloud droplets (i.e., constant droplet number concentration in the vertical, and monotonically increasing LWC and r_e). More discussion on the applicability of the adiabatic assumption is available in Grosvenor et al. (2018).

Furthermore, when assuming adiabatically ascending air parcels within a cloud, N_d can be expressed as (Grosvenor et al., 2018)

$$N_d = \frac{\sqrt{5}}{2\pi k}\left(\frac{f_{ad} c_w \tau_c}{Q_{ext}\rho_w r_e^5}\right)^{1/2} \tag{5}$$

The adiabatic fraction, f_{ad}, is usually assumed as 1, while actually, it is mostly much less than 1 (typically between 0.1 and 0.9). c_w is the condensation rate, k is the PSD width parameter (about 0.8), Q_{ext} is the average extinction efficiency factor ($Q_{ext} = 2$), and ρ_w the liquid water density. The reader can refer to Grosvenor et al. (2018) for a complete derivation of the equation and a thorough discussion of uncertainties related to this approach. The review paper of Grosvenor et al. (2018) estimates an overall error on N_d about 78% for single-layer stratocumulus cases, where the adiabaticity assumption is most reasonable and clouds are spatially homogeneous. Gryspeerdt et al. (2022a) showed through comparisons to in-situ observations of single-layer marine Sc that this uncertainty can be reduced to 30%–50% depending on the data filtering strategy and potentially further through spatial aggregation.

Bi-spectral satellite cloud property retrievals, as shown in Figure 5, commonly assume plane-parallel homogeneous water clouds. In reality, not all clouds can be approximated by plane-parallel layers. They can have various shapes and can be internally inhomogeneous for both LWC and r_e. In addition, the clouds are mostly sub-adiabatic at various extents, while Equation 5 requires knowledge of the adiabatic fraction. Since the adiabatic fraction is not yet available from satellite measurements it is often assumed as 1 when using Equation 5. Another cause for errors is the fact that the radius of water droplets can decrease near the cloud top. Therefore, the satellite-derived value of r_e is representative of the value close to the cloud top within a few optical depths (Platnick, 2000). The derived COT is a more robust cloud property because the optical thickness is contributed equally from the full depth of the cloud.

Since the cloud reflectance tends to saturate in very thick clouds, the accuracy of the determination of COT decreases with the increasing value of τ_c, limiting the values of satellite-derived τ_c to 100 or so. Therefore, both LWP and τ_c cannot be determined for very thick (e.g., cumulonimbus) cloud systems using optical observations. The same is true for optically thin cloud layers, where the parameters τ_c and r_e are no longer orthogonal (see example in Figure 5) and so cannot be determined independently. This occurs below τ_c around 2–3, where the internal cloud inhomogeneity (e.g., LWC spatial variation) is rather large and clouds cannot be adequately modeled as homogeneous plane-parallel layers. For small τ_c the underlying surface reflection also has a substantial impact on the measured reflectances, which represents an important source of error. For this reason, MODIS retrievals over land use the 670 nm band, which has a relatively low surface reflectance.

The biases due to cloud inhomogeneity and small τ_c issues can be avoided by the use of polarimetric measurements at scattering angles in the range 135°–165°, where the primary and secondary cloud bows for water droplets occur (Alexandrov et al., 2012). Here, polarized reflectance as a function of scattering angle depends

strongly on the r_e and v_e of the PSD. This methodology provides a calibration error-free r_e, ν_e, or even the full PSD (Alexandrov et al., 2012b). For POLDER operational processing, cloud bow retrievals have been performed for large super-pixels to increase angular resolution (Bréon & Colzy, 2000). More recently, cloud-bow retrievals have been performed at the POLDER native resolution of 6×6 km^2 (di Noia et al., 2019). Polarimetric cloud retrievals provide the cloud effective radius close to the top of the cloud (within 1 optical depth), where cloud drops tend to become smaller by evaporation. As such, the polarimetric-retrieved r_e is smaller than the bispectral-retrieved r_e (Breon & Doutriaux-Boucher, 2005), which may lead to a smaller susceptibility to aerosols (Rosenfeld & Feingold, 2003). Improved polarimetric cloud retrievals for ACI studies are expected from HARP-2 on the NASA PACE mission (Werdell et al., 2019) which has a higher angular resolution than POLDER (60 angles vs. 15 for POLDER). However, the relatively large pixel size of HARP-2 (5×5 km^2) makes the interpretation of the retrieved r_e difficult for cloud fields with strongly varying cloud tops (and hence r_e) within a pixel.

High-resolution r_e-retrievals can currently only be performed using the bi-spectral method. In this respect, the usage of EnMAP (https://www.enmap.org/mission/) and PRISMA (https://www.eoportal.org/satellite-missions/prisma-hyperspectral#performance-specifications) hyperspectral (30 m spatial resolution) satellite missions could lead to a better understanding of ACI and aerosol-mediated cloud forcing. In particular, EnMAP performs measurements at 224 channels in the range 418–2,445 nm and PRISMA makes measurements in the spectral range 400–2,505 nm (237 channels). Both missions feature main channels commonly used for aerosol and cloud retrievals based on the measurements performed by MODIS and provide additional advantages both for aerosol and cloud remote sensing (e.g., estimation of aerosol and cloud top altitudes). The respective algorithms are currently under development. A limitation of high-resolution bi-spectral retrievals is their sensitivity to three-dimensional radiative transfer effects. A potential way forward for the next generation of satellites is to perform high spatial resolution multi-angle polarimetric observations.

Retrievals of r_e and N_d can be done also based on the CALIOP space-borne lidar, relaying on the radiation extinction and depolarization rates at the cloud tops. This method is not used extensively due to the poor coverage of the CALIOP (Y. Hu et al., 2007; S. Hu et al., 2021, Y. Hu et al., 2021).

Another important parameter of cloud layers, needed for ACI studies is the actual position of cloud layers in the atmosphere (base and top heights, geometrical thickness, number of layers, horizontal variation of cloud layers' extent) and the position of cloud layers with respect to aerosol layers (say, dust outbreaks, smoke, etc.). From a passive remote sensing perspective, the cloud top height can be derived from measurements in the thermal IR of CO_2 bands or from oxygen A-band spectrometry. The idea behind the method is the fact that the differential attenuation between the oxygen and nearby non-absorbing band as a function of height is known. Cloud top height can be obtained also by the combined retrieved cloud top temperature and a sounding of the vertical temperature profile. The most accurate information on cloud vertical distribution can be derived from lidar and radar observations, including cloud base height (CBH) at an accuracy of $\pm$115 m (X. Lu et al., 2021), which improved a similar methodology of Mülmenstädt et al. (2018). This methodology is looking for the lowest CBH along a segment of several tens of km. It identifies a cloud base if the cloud is sufficiently penetrable for detecting the lidar surface reflection. It works only for broken or very thin clouds. Cloud base height products for liquid clouds are also available from multi-angular observations (Böhm et al., 2019).

Cloud fraction, f, is another important cloud property needed to quantify ERF_{aci}. Most cloud retrievals work under the assumption that a satellite pixel of a typical size of 1 km is 100% covered by clouds. The value of f is then determined for a larger area by using the number of cloudy and cloud-free pixels in that area. The assumption that a pixel is either 100% cloudy or cloud-free becomes more reliable for higher spatial resolution measurements, such as 375 m of the Visible Infrared Imaging Radiometer Suite (VIIRS) imager. It is also possible to retrieve f within a satellite pixel from measurements based on the scattering and absorption optical thicknesses in two different absorbing wavelength bands in the UV and NIR (van Diedenhoven et al., 2006).

The main cloud parameters retrieved using remote techniques are summarized in Table 1.

3.2. Aerosol Properties

Atmospheric air contains a variety of solid and liquid particles of various chemical compositions, sizes, and concentrations. Usually, a distinction is made between at least two size modes of particles in the atmosphere—fine and coarse modes, separated at a diameter of 1 μm. The chemical composition and origin of the modes

Reviews of Geophysics

10.1029/2022RG000799

Table 1
Retrieved Cloud Parameters

Cloud parameter	Typical measurement range and uncertainty	Comments
r_e, Effective radius	4–30 μm; 8%	Passive measurements provide value at the cloud top
COT, Cloud optical thickness (at 550 nm)	1–100; 10%	Can not be retrieved for thick clouds with COT > 100 or so
LWP, cloud liquid water path	10–500 gm^{-2}; 15%	This quantity together with the value of r_e can be used to identify precipitating clouds
N_d, Cloud drop number concentration	10–1,500 cm^{-3};30%	For passive retrievals, N_d is typically inferred from the retrieved r_e and COT under the adiabatic assumption
$N_{d\text{-}ad}$, Adiabatic cloud drop number concentration	10–1,500 cm^{-3}; 30%	Retrieved by assuming an adiabatic r_e and matching it to the adiabatic LWC (Rosenfeld et al., 2016)
CBH, Cloud base height	0.2–20 km; 150 m	CBH can be derived from lidar, radar, thermal infrared
CBT, Cloud base temperature	−10 to 27°C; 1.1°C	CBT can be derived from thermal infrared Zhu et al., 2014)
CTH, Cloud top height	0.2–20 km; 100 m	CTH can be derived from lidar observations, thermal infrared, or oxygen A-band spectrometry
CGT; Cloud geometrical thickness	0.2–20 km; 200 m	CGT can be derived from lidar or radar observations and also from oxygen A-band spectrometry
f, Cloud fraction	0–1; 0.2	Satellite imagery
Cloud thermodynamic phase	Water, ice and mixed clouds	Spectral measurements in the vicinity of water and ice absorption bands are needed; Light depolarization measurements
W_b, Cloud base updraft	0.1–3 ms^{-1}; 27%	W_b is derived from cloud top radiative cooling rate derived from radiative transfer modeling and from CTH and reanalysis sounding (Zheng et al., 2015). Also derived from CBH (Zheng et al., 2016)
S_b, Cloud base supersaturation	0.1%–1%; 25% of S_b	S_b is derived from N_d and W_b (Rosenfeld et al., 2016)
N_{CCN}, Cloud base CCN at S_b	10–1,500 cm^{-3}; 30%	N_{CCN} is the adiabatic N_d at the supersaturation S_b

Table 2
Aerosol Properties Retrieved Using Remote Sensing Techniques

Aerosol parameter	Symbol	Typical range	Required uncertainty
Effective radius of the fine (coarse) mode	$a_{ef,f}$ $a_{ef,c}$	0.05–0.5 μm (fine)/0.5–5.0 μm (coarse)	10%
Effective width of the fine (coarse) mode	$\nu_{ef,f}$ $\nu_{ef,c}$	0.10–0.4 (fine)/0.4–0.8 (coarse)	50%
Complex refractive index of the fine (coarse) mode	$n_f - i\chi_f$ $(n_c - i\chi_c)$	Real part: 1.33–1.60/imaginary part 10^{-9}–0.2	Real part: 0.02
Particle column fine mode	C_f	10^{10}–10^{13} m^{-2}	10^{11}
Particle column coarse mode	C_c	10^{7}–10^{11} m^{-2}	10^{9}
Relative concentration of nonspherical particles in coarse mode	C_{cns}	0–1	–
Geometrical parameters of aerosol layer (thickness, top and bottom heights)	ΔH, H_{bot}, H_{top}	Depend on aerosol layer origin (fires, volcanic eruption, dust outbreaks, etc.)	500–1,000 m on H_{top}

Note. For the definition of fine- and coarse mode we assume the aerosol size distribution can be described by the summation of a number of log-normal function, called modes. Modes for which the effective radius is smaller/larger than 0.6 micron are referred to as fine/coarse mode. Required uncertainties (where available) are based on Mishchenko et al. (2004), Hasekamp et al. (2019a), and the Global Climate Observing System (GCOS) implementation plan 2016.

and, therefore, spectral refractive index differ. Both the fine and coarse modes may contain irregularly shaped particles (e.g., soot or dust). One can use various models of non-spherical particles for modeling their light. T-matrix calculations for spheroids can also be used. Most retrieval algorithms that take particle non-sphericity into account make use of the Mie- and T-matrix improved geometrical optics database by Dubovik et al. (2006) to compute the optical properties of a mixture of spheroids and spheres.

An aerosol retrieval algorithm for space-borne observations should account for the characteristics of aerosol particles that are given in Table 2. It depends on the information content of the measurements and the retrieval algorithm to what extent these properties are retrieved independently or rely on prior assumptions. For aerosol retrieval from multi-spectral radiometric observations, the most common approach is the minimization of differences between measured reflectances and atmospheric reflectances stored in look-up-tables (LUTs) for different spectral channels and viewing geometries. The reflectances in the LUT are computed for several standard aerosol models, where a model represents a certain combination of aerosol properties in Table 2, based on prior information for different aerosol types. For aerosol retrievals from multi-spectral, multi-angle measurements of radiance and polarization, the information content allows retrievals of most parameters of Table 2 independently (Hasekamp & Landgraf, 2007; Knobelspiesse et al., 2012). Such retrievals do not have to rely on aerosol models but can consider a continuous parameter space for the different aerosol properties, and can retrieve surface properties simultaneously with aerosol properties (Dubovik et al., 2011; Fu et al., 2020; Hasekamp et al., 2011). The corresponding retrieval algorithms are based on the minimization of the differences between the measured values for radiance and polarization and online radiative transfer calculations. It is assumed in the retrievals that the aerosol layer can be represented by a plane-parallel vertically and horizontally homogeneous light scattering and absorbing turbid medium. In some cases (e.g., using lidar techniques or a combination of active and passive remote sensing techniques) the profiles of respective aerosol parameters can be derived.

The quantities presented in Table 2 can be used to derive the spectral AOD, which is the column-integrated aerosol extinction, and the single scattering albedo, which is the ratio of scattering efficiency to total extinction efficiency. The wavelength dependence of the AOD can be approximated by Equation 6:

$$\tau_a(\lambda) = \tau_a(\lambda_0)(\lambda/\lambda_0)^{-A} \quad (6)$$

where A is the Angström Exponent (AE). The AE gives an indication of particle size, where small AE values (AE < 1) correspond to large particles and large AE values (AE > 1.5) to small particles. The accuracy of retrievals deteriorates with increasing underlying surface reflectance (e.g., bright surfaces—snow, ice, and deserts).

Besides microphysical- and optical aerosol properties, also the vertical profile of aerosols is important. The most detailed information on the aerosol vertical profile can be obtained from lidar observations (Lopatin

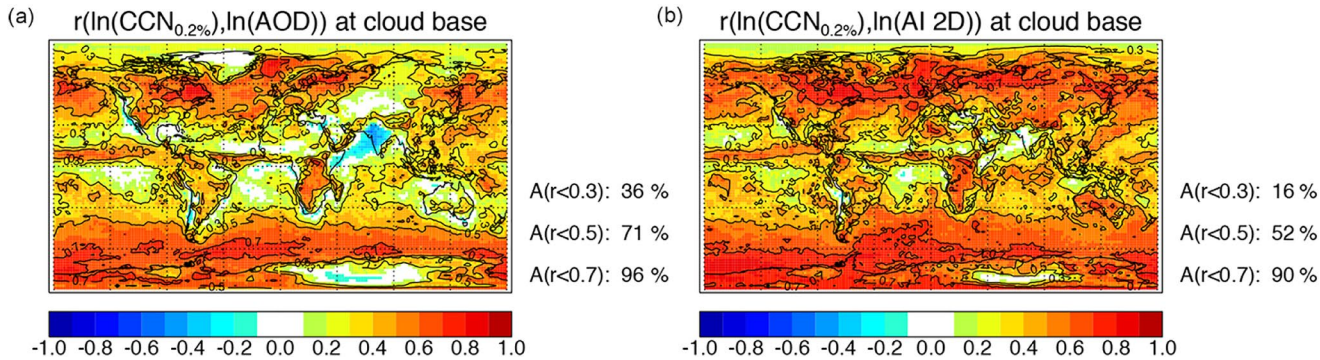

Figure 6. Global map of the correlations between the simulated perfectly retrieved aerosol optical depth (a) and Aerosol Index (b) with cloud base cloud drop condensation nuclei at $S_b = 0.2\%$. The text to the right of the panels shows the global area percentage for which the correlation is smaller than 0.3, 0.5, and 0.7, respectively. From Stier (2016). Note that the area of lowest correlation coincides mostly with the ocean areas that are subject to large variability from anthropogenic aerosols.

et al., 2013, 2021). From passive measurements, an aerosol layer height can be retrieved using polarimetric measurements in the near UV or spectrally resolved radiometric measurements in the O_2 A-band.

3.3. Aerosol Optical Properties as Proxies for CCN

Assuming a single size, shape, and chemical composition of particles, AOD is considered to be a first-order proxy for column CCN concentrations at fixed supersaturation (Andreae, 2009). Aerosol optical depth has been thus widely used in satellite-based studies of ACI (e.g., Bellouin et al., 2020). However, for realistic aerosol distributions, the aerosol microphysical properties vary significantly over space and time, not fully satisfying the fundamental assumption made for using AOD. Another similar proxy for CCN is fine-mode AOD (AODf), which can be directly retrieved from satellites (e.g., MODIS, MISR, and POLDER). To further refine this idea, the new polarimetric aerosol retrievals with the information on the aerosol number, size, and shape, are employed to infer column CCN concentrations, considering the impacts of both particle size and hygroscopicity (Hasekamp et al., 2019b).

The distinct effects of coarse- and fine-mode aerosols on cloud droplet size are further challenges for this assumption (F. Liu et al., 2022). A modeling study suggested that perfectly retrieved AOD variability explains less than 25% of the $CCN_{0.2}$ (CCN that activates cloud droplets at $S_b = 0.2\%$) variance for 71% of the area of the globe (Stier, 2016). Furthermore, the AI, which is the product of AOD and AE, is a better proxy for column CCN, as it gives lower weight to large-size aerosol (e.g., sea salt and dust particles) that contributes substantially to extinction but slightly to number concentration (Nakajima et al., 2001). The AI variability still explains less than 25% of the $CCN_{0.2}$ variance for 53% of the area of the globe, representing some improvement compared to the 71% for AOD (Stier, 2016) as shown in Figure 6.

Modeling studies concluded that compared to AOD–N_d relationships, AI–N_d relationships are better for predicting the present-day—preindustrial change in N_d (Gryspeerdt et al., 2017; Penner et al., 2011), since it better accounts for the differing present-day and preindustrial aerosol environments. This, in turn, applies also to AODf and column CCN concentrations.

However, none of the above proxies can get rid of the lack of horizontal and vertical colocation of aerosol and N_d retrievals. The horizontal colocation requires the simultaneous retrievals of aerosol and N_d at least on a coarse-resolved grid (such as 1 by 1° on a latitude-longitude grid), in which aerosol retrievals in clear pixels are assumed to be representative of aerosol under cloudy pixels (Anderson et al., 2003a, 2003b). Nevertheless, when clouds fully cover the large grid box, hampering any aerosol retrievals from their optical signal, these clouds are not sampled for statistical analysis. This sampling bias tends to discard retrieval-reliable stratiform clouds that are more sensitive to aerosol perturbations. Furthermore, added aerosols may increase the cloud fraction to a full cloud cover (Rosenfeld et al., 2019). Excluding such clouds would underestimate the overall CF sensitivity and RF_{aci} (Jia et al., 2021). To overcome this problem, one can make use of aerosol products from data assimilation systems (reanalysis) that are constrained by satellite-retrieved aerosol properties that are available everywhere in

Table 3
The Main Satellite Instruments and Their Retrieved Proxies for Cloud Drop Condensation Nuclei (CCN), and Their Relative Advantages and Disadvantages

CCN proxy	Instruments	Comments
AOD	MODIS, VIIRS	Insensitive due to the disproportionate effect of large aerosols thus causing an underestimation of the susceptibility (Penner et al., 2011). Even a perfectly retrieved AOD variability explains less than 25% of the $CCN_{0.2}$ due to uncertainty in vertical distribution (Stier, 2016)
Fine and coarse AOD fraction	MODIS, VIIRS, MISR	Useful for improved CCN and GCCN proxies. Still not as good as Aerosol Index as a CCN proxy. AOD swells with relative humidity and distorts the relationship with CCN
Aerosol Index	MODIS, VIIRS	Better than AOD as it gives lower weight to large size aerosol (Nakajima et al., 2001)
AOD, r_e, Type	POLDER, PARASOL	Can convert the measurements of aerosol size and composition (Dubovik et al., 2019a, 2019b) to column CCN (Hasekamp et al., 2019b). Still vertical uncertainty
Aerosol type, backscatter, extinction, height	CALIOP	Lidar, provides aerosol height, which is critically important to collocate with the cloud base height. Winker et al. (2009)
N_d of cloud tops	MODIS, VIIRS	Direct relationship to CCN in aerosol-limited conditions. N_d for the same CCN decreases sharply with height above the cloud base, especially in precipitating clouds (Efraim et al., 2020)
CCN(S_b)	VIIRS	Retrieved cloud base adiabatic N_d and updraft provide supersaturation S_b, so the N_d is CCN(S_b). Accuracy of ±30%. Rosenfeld et al. (2016). Fails in updraft-limited conditions or when GCCN dominates

space and time (Jia et al., 2021; McCoy et al., 2017). Data assimilation systems typically make only use of satellite-retrieved AOD (e.g., Inness et al., 2019), but recent studies also make use of observations of aerosol size and absorption (Tsikerdekis et al., 2021, 2022).

On the other hand, vertical colocation requires aerosol information at the cloud base, which is possible from either active lidar observations or aerosol reanalysis. A study using CALIOP observations found a lower correlation between N_d and AOD compared to N_d versus aerosol extinction coefficients at cloud base (Painemal et al., 2020), in line with the finding from a modeling study (Stier, 2016). A new CCN retrieval from CALIPSO lidar measurements (Choudhury & Tesche, 2022) provides vertically resolved CCN concentrations, which is a promising future direction. However, it is noted that the vertical observations from active lidar still suffer from the sampling bias toward measurements in clear skies. The use of reanalyzed aerosol profile can sidestep this issue, although without measurements to constrain their behavior in cloudy skies, care must be taken in their use (Grandey et al., 2014). In addition, the available operational aerosol re-analyses do not yet assimilate lidar measurements, with current lidar measurements (CALIPSO) suffering from low sensitivity (P. L. Ma et al., 2018; X. Ma et al., 2018; Watson-Parris et al., 2018). Even with these issues, using column-integrated sulfate to approximate sulfate near the cloud base leads to a nearly twofold enhancement of the N_d sensitivity (Jia et al., 2022). This is attributed to the inability of column aerosol to capture the full spatiotemporal variability of cloud base aerosol (Jia et al., 2022). In contrast, the sulfate near the surface behaves quite similarly to cloud base sulfate in terms of both correlation coefficients and N_d sensitivity (Jia et al., 2022).

The use of different CCN proxies results in diverse estimations of N_d susceptibilities from satellites. Among column CCN proxies, typically, the largest N_d susceptibilities are found for column CCN, followed AI and AODf, with the smallest susceptibilities found when using AOD (Gryspeerdt et al., 2022a; Hasekamp et al., 2019b; Jia et al., 2021, 2022). With respect to the vertical co-location, the N_d susceptibility from column-integrated proxies is nearly twice as large as those from proxies at the cloud base and surface (Jia et al., 2022). However, it is important to note that the sensitivity alone does not determine the utility of the proxy for calculating the ERF_{aci}, where we are primarily concerned with the PD–PI change in N_d (relevant to radiative forcing, Equation 3). For example, it has been shown by Gryspeerdt et al. (2017) that column-integrated CCN concentrations or AI are able to adequately predict the PI-PD change in N_d and hence RF_{aci}, provided they are retrieved accurately. This requires the same aerosol quantity to be used for the aerosol-N_d sensitivity and the PI-PD aerosol change because the larger N_d sensitivities from column-integrated proxies are being compensated by a smaller anthropogenic fraction compared to cloud base proxy. The above issues raise complications to compare and reconcile the diverse N_d sensitivities. The choice of an adequate quantity for cloud-active aerosol and the corresponding accuracy are crucial factors that determine most of the uncertainty in RF_{aci} estimates (Gryspeerdt et al., 2022a) (Table 3).

In summary, satellite-retrieved optical properties of aerosols as a proxy for CCN concentration at cloud base have the following capabilities and limitations for studying ACI:

(a) The AOD-N_d relationship is not suited to diagnose ΔN_d because aerosols swell at high relative humidity and therefore increase the AOD and decrease the AE for the same CCN concentrations (Boucher & Quaas, 2013; Kapustin et al., 2006). In addition, the PD-PI difference in AOD is not representative of the anthropogenic CCN perturbation.

(b) The AI-N_d relationship is much better suited to diagnose ΔN_d if it can be retrieved with very high accuracy. The reason is that AI is a better proxy for cloud-active aerosol in Equation 1 (Gryspeerdt et al., 2017). However, AI retrievals have large uncertainties, especially in clean conditions and over land. The CCN activity of the aerosols may also vary for the same AOD and AI, depending on the solubility and size distribution (J. Liu & Li, 2014).

(c) Relating a CCN proxy based on retrieved size distribution and number concentration from polarimetric measurements, to N_d has a better capability to diagnose ΔN_d than using relationships based on AOD and AI. Current products have limited accuracy under clean conditions (although better than AI) and over land.
(d) Aerosol particles $< \sim$100 nm are usually not detected by the optical remote sensing instrumentation, but can still contribute most of the CCN under some conditions.
(e) Clouds contaminate the AOD and AI signals, as these signals are measured in cloud-free areas near the clouds (Koren et al., 2008).
(f) The aerosols that affect clouds are near the cloud base, but they are obscured from the satellite view by the very clouds that they interact with.
(g) Clouds, especially non-precipitating ones, detrain the aerosols aloft where cloud droplets evaporate, thus increasing the AOD for the same boundary layer CCN concentrations. This might produce a non-causal positive correlation between cloud geometric thickness (CGT) and AOD.
(h) The optical signal of the aerosols for current satellites vanishes to the noise level in clean marine environments where N_d reaches 35 cm^{-3}, on average (Hasekamp et al., 2019b). Much of the ocean areas have $N_d \leq 35$ cm^{-3}, for which a small absolute change in CCN makes a large fractional change in N_d and R_{cld}, respectively (Carslaw et al., 2013).

3.4. CCN Derived From Retrieved Cloud Properties

The N_d-CCN relationships at the level of an individual air parcel have been known for a long time (Köhler, 1936; Twomey, 1959). The hygroscopicity parameter, kappa (Petters & Kreidenweis, 2007), provided a practical way for converting the aerosol size distribution and composition into the aerosol CCN activity. The advent of satellite retrieval of cloud base updraft (Zheng, 2019; Zheng et al., 2015, 2016) and cloud base adiabatic drop concentrations, $N_{d\text{-}ad}$ (Efraim et al., 2020; Rosenfeld et al., 2016; Wang et al., 2021), made it possible to retrieve cloud base supersaturation, S_b, thus allowing to infer CCN concentrations from the retrievals of updraft and $N_{d\text{-}ad}$. This is based on the calculation of cloud base supersaturation, S_b, as given by Pinsky et al. (2012):

$$S_b = C(T_b, P_b) W_b^{3/4} N_d^{-1/2} \quad (7)$$

where C is a coefficient that depends weakly on cloud base temperature (T_b) and pressure (P_b). Then, the satellite-retrieved N_d is the CCN concentration at S_b. The satellite CCN retrievals were validated by comparisons to shipborne CCN (Efraim et al., 2020; Rosenfeld et al., 2016; Wang et al., 2021). The accuracy of the retrieved CCN based on the retrieved $N_{d\text{-}ad}$ is estimated at ±30% and explained 76% of the variability of the whole data set (Efraim et al., 2020; Rosenfeld et al., 2016; Wang et al., 2021). An example of maps of retrieved N_{CCN}, W_b, and S_b is shown in Figure 7.

The advent of retrieval of $N_{d\text{-}ad}$ made it possible to bridge between the susceptibility of the retrieved N_d-CCN relationships at the scene level and the susceptibility of unity (by definition) of the $N_{d\text{-}ad}$-CCN relationships at the parcel level. It should be noted that retrieval of $N_{d\text{-}ad}$ retrieved by the methodology of Rosenfeld et al. (2016) is not affected by the adiabatic fraction. The methodology retrieval of $N_{d\text{-}ad}$ of Efraim et al. (2020) and Wang et al. (2021) provides Equation 5 with the average adiabatic fraction dependence on cloud depth. This improved the accuracy of retrieved N_d to ±30%.

In a similar approach, Saide et al. (2012) have proposed the combination of models with cloud observations to infer below-cloud CCN concentrations. An advantage of this methodology is that it removes the uncertainty of the satellite retrieved aerosol properties and their conversion to proxies of CCN, but on the other hand retrieval uncertainties in N_d now propagate into the retrieved CCN concentration. Another uncertainty of retrieving N_d remains the same for both methods. An added uncertainty is in the retrieval of cloud base updraft, which is estimated at 27% (Rosenfeld et al., 2016). Since for updraft limited conditions, N_d increases with $W_b^{0.5}$ (Twomey, 1959), the error in the retrieved N_d is inversely proportional to the square root of the error in the updraft. When approaching aerosol-limited conditions the inaccuracy in the updraft speed matters less. Application of this updraft bias correction to the retrieved N_d showed little change in the resultant susceptibilities of cloud properties to N_d (Rosenfeld et al., 2019).

The anthropogenic perturbation of aerosols cannot be observed directly but must be simulated with actual natural and anthropogenic emission sources, using a model that can reproduce the perturbation, calculating the CCN concentrations with and without the anthropogenic emission sources. The simulations have to include the major

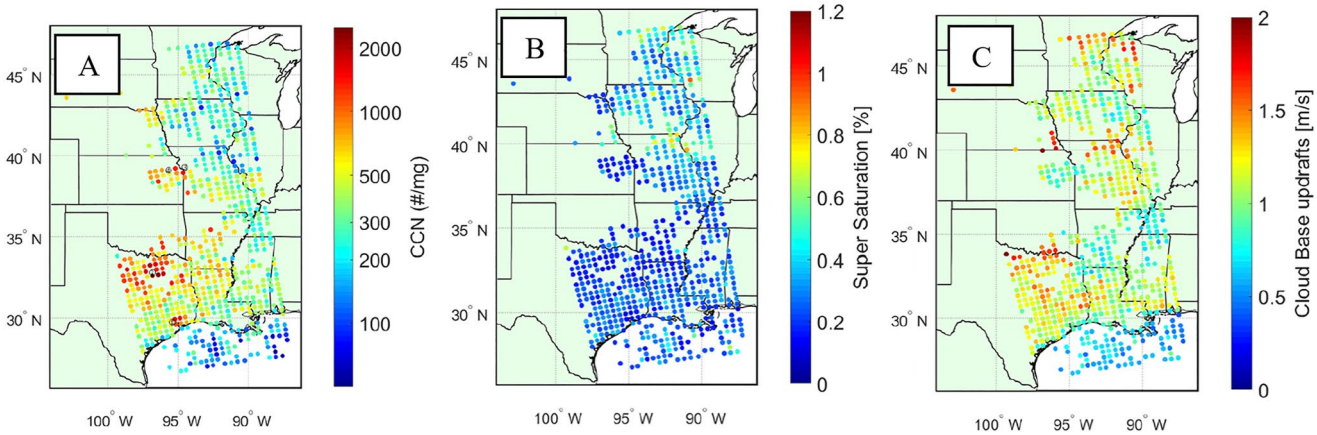

Figure 7. Satellite-retrieved cloud drop condensation nuclei (CCN) based on the imager channels of the Visible Infrared Imaging Radiometer Suite onboard the Suomi National Polar-orbiting Partnership satellite on 1930 UTC 30 July 2016. The components are the CCN number concentrations (a) at the cloud base maximum supersaturation shown in (b), caused by a cloud base updraft speed shown in (c). The signature of major cities such as Houston, and Dallas are evident as elevated levels of CCN. From Yue et al. (2019).

processes of aerosol formation by the various mechanism, growth, chemical evolution, transport, deposition, cloud processing, and wet scavenging. The simulations can be validated and constrained against satellite-retrieved maps of CCN. Such CCN maps and their components (cloud base N_d, updraft speed, and vapor supersaturation) can be generated as demonstrated by Yue et al. (2019) and Z. Liu et al. (2020), as shown in Figure 7. The uncertainty of the retrieved CCN can be measured by the differences between the satellite retrievals and in situ or surfaced-based measured cloud base N_d and updrafts (Efraim et al., 2020; Fanourgakis et al., 2019; Rosenfeld et al., 2016; Wang et al., 2021).

From the aerosol side, it is required that simulations of natural and anthropogenic CCN are representative of the observed clouds, that is, weather patterns and model resolution have to match the satellite observations. From the cloud side, it is required that the simulations will resolve the convective cloud updrafts. Resolving the updrafts is strongly dependent on the spatial resolution. The lacking of proper updrafts in GCMs was already recognized as a possible "key to unlocking climate forcing and sensitivity" (Donner et al., 2016; P.-L. Ma et al., 2015). Simulations that combine a full representation of the known aerosol effects on deep convective clouds at a global multi-annual scale are not yet available.

In summary, satellite retrievals of W_b and $N_{d\text{-}ad}$ represent new emerging possibilities, based on a different set of assumptions to optical retrievals of aerosol properties. However, they have their limitations which include:

(a) Reliance on N_d retrieval, which has significant uncertainties, particularly for inhomogenous scenes.
(b) Uncertainties in cloud base updrafts, which add to the uncertainties in retrieving N_d. The combined inaccuracies of the calculated CCN from N_d and W_b are estimated at ~30%.
(c) Using this methodology for calculating radiative forcing requires the GCMs to calculate explicitly the changes in CCN and W_b, which is yet an unresolved challenge.

4. General Issues

4.1. Aggregation Issues

Cloud properties vary at all scales and respond to both aerosols and meteorological cloud-controlling factors. Furthermore, important differences in aerosols, cloud-controlling factors, and satellite retrieval capabilities occur over different types of surface areas, especially between land and ocean. The differences in cloud and aerosol properties under these different conditions are discussed in this section, as well as the need and ways to aggregate clouds under similar meteorological cloud-controlling factors.

4.1.1. Spatial Aggregation

According to Section 2, there are two main kinds of regimes used to classify clouds. "Cloud regimes" are based on the observed properties of the cloud, such as cloud fraction and precipitating state. "Meteorological regimes" are defined by the cloud-controlling factors, which include LTS and inversion height, relative humidity, and

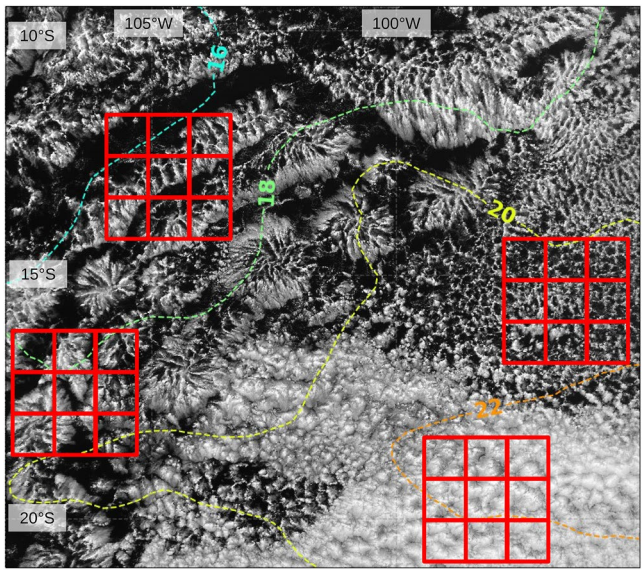

Figure 8. Visible satellite image of the scale hierarchy of self-aggregation of marine stratocumulus. The visible image was taken by MODIS Terra on 21 July 2019, 20:30 UTC. The small rectangles cover an area of 1 × 1 degrees, whereas a group of 9 rectangles covers an area of 3 × 3 degrees. The dashed lines represent the low tropospheric stability (LTS) (°C). Each 3 × 3 degree scene represents a rather homogenous cloud appearance regime (from east to west: open cells, closed cells, fish, and flowers). However, the transitions between these regimes appear poorly correlated to the LTS. When considering a single 1 × 1 degree sub scene, the regional cloud regime cannot be distinctly determined (see, e.g., that 1 × 1 degree scenes in every regime be clear, partially cloudy, or fully cloudy, regardless of the CF of the entire 3 × 3 degree scene). To obtain a representative cloud fraction, spatial aggregation must be aggregated within the spatial scale of cloud-controlling factors.

vertical motion of the free troposphere. The scale of spatial variability of the cloud-controlling factors may be larger than the spatial scale of the cloud properties, as evident in Figure 8 (after Figure 1 of Rosenfeld et al., 2019). Furthermore, the cloud properties can be strongly affected by aerosols, leading to transitions between cloud regimes of open and closed MCC, without much change in cloud-controlling factors. It is an open question whether aerosols affect the transitions between fish, gravel, sugar, and flowers as used by Stevens et al. (2020a, 2020b). All these cloud regimes are evident in Figure 8, while the cloud-controlling factors within the domain are rather homogeneous.

If the regime integration of Equation 3 is done using meteorological regimes and the spatial scale of these regimes is often larger than the cloud regimes, the cloud data have to be aggregated for the bins of the cloud controlling factors, as was done by Koren et al. (2005), Rosenfeld et al. (2019), and by Bony et al. (2020). The cloud properties are typically aggregated in gridboxes of 1 × 1 degrees, as shown in Figure 8. The 3 × 3 degree matrices demonstrate that the cloud fraction can vary greatly between 1 × 1 degree areas while keeping even in the same cloud regime, such as flowers.

The spatial aggregation errors due to too small grids can be overcome by averaging the CF and other properties of many such scenes of the same meteorological regime, as done by Koren et al. (2005) and Rosenfeld et al. (2019) for 1 × 1 degree scenes.

4.1.2. Temporal Aggregation

Similar to spatial averaging, data are often averaged over periods ranging from instantaneous, in which MODIS Terra and Aqua observations single overpass time are taken, to daily, and up to a month (e.g., MODIS L3 monthly data, Y. Chen et al., 2022). This may lead to averaging different types and regimes of clouds into a single value, an issue that is most pronounced in regions with large variances in the climatological and aerosol means. Therefore, it is important to ensure that the temporal average will not exceed 24 hr, a period that exceeds the typical lifetime of a cloud system (Dagan et al., 2018) and the aerosol temporal decorrelation time (Rosenfeld & Woodley, 2003), which is less than 24 hr. Averaging beyond the time or space scales of the aerosols and/or cloud regimes would average out the variability and therefore might result in an erroneously reduced susceptibility. However, susceptibilities must be calculated over large enough spatial area or temporal domain to ensure sufficient variation in the independent variable.

Figure 9 demonstrates the effect of temporal and spatial aggregation on the sensitivity of the LWP to N_d. Figures 9a and 9b show that 2-day sensitivities produce a positive relationship, which becomes negative when the averaging period is extended beyond 5–10 days (panel c). This may be a manifestation of Simpson's paradox (Feingold et al., 2022). Panel c further shows the dependence on the spatial aggregation resolution, with larger aggregation scales tending to lower sensitivities. Conversely, at too small temporal and spatial scales, the small variation in N_d used for calculating the sensitivities may lead to an erroneously positive sensitivity, driven by optical depth variations across a single cloud, with the response to aerosol variations only becoming visible at larger spatial and temporal scales. The optimal scale should encompass the full lifecycle of a cloud cluster in time and space, but not much larger than that.

4.1.3. Regime Aggregation

The ERF_{aci} is linearly correlated with the weights of occurrence of the regimes which are integrated in Equation 3. Similar susceptibilities among different studies generally imply a smaller uncertainty of the global ERF_{aci}. However, without similar occurrences of these regimes, the reduced uncertainty is not guarantee. When comparing global ERF_{aci} estimates among studies it is therefore crucial that the occurrence terms be comparable, or at least scaled to be comparable to the extent possible. This requires the studies to provide a detailed description of the exact filters that were applied to the data from which the cloud occurrences were derived.

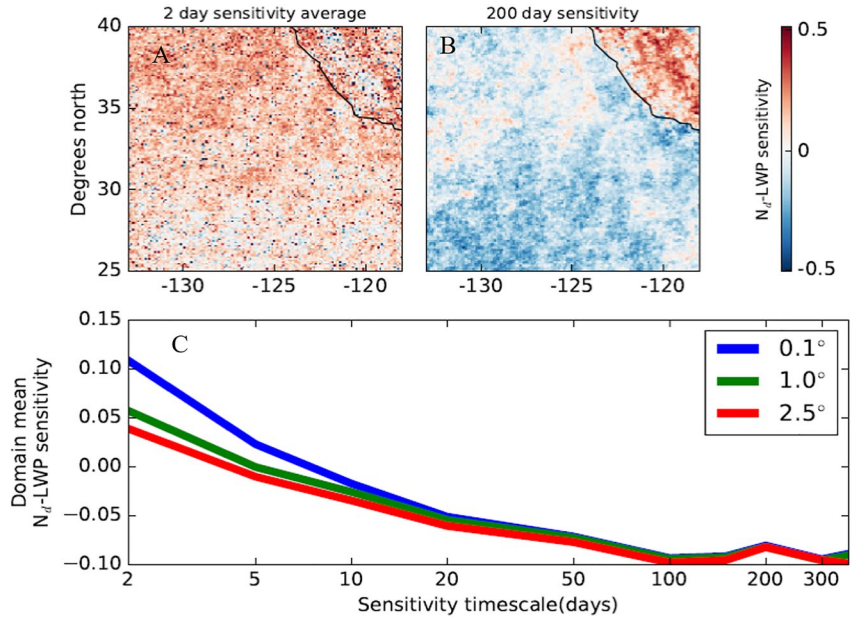

Figure 9. The dependence of the susceptibility of liquid water path (LWP) to N_d on the averaging time scale. The susceptibility of LWP to N_d is shown to become smaller over longer averaging times of LWP and N_d. It is shown spatially (a, b) and temporally (c). The figure was created using data from Gryspeerdt et al. (2019).

4.2. Retrieval Sampling Biases/Climatological Representativeness

Uncertainties in the retrieved MODIS cloud microphysical properties are mainly due to partial pixel filling by clouds and three-dimensional radiation effects, which are more common at cloud edges and broken clouds (Loeb & Manalo-Smith, 2005; Wen et al., 2007; J. Zhang et al., 2005). To avoid such biases, a threshold COT and r_e are often applied (Sourdeval et al., 2015). This leads to (a) the exclusion of unquantified and potentially significant cloudy pixels from the scene means and (b) a high bias of the scene mean microphysical properties due to the exclusion of the thinner clouds.

Furthermore, failed cloud retrievals that occur when there is no combination of optical thickness and r_e in the MODIS look-up tables that can explain the observed cloud reflectance produce an additional bias (Goren et al., 2018). As an example, the leading type of such a retrieval failure is due to an r_e that is too large, outside the range of MODIS look-up tables, which are limited to 30 μm (Cho et al., 2015). This problem occurs also in the VIIRS products. Such a failure is common in convective cores of heavily precipitating broken shallow clouds, where the r_e can increase to such values due to strong updrafts that prevent the drops from falling. This means that heavily precipitating clouds with r_e greater than 30 μm are not represented in the standard cloud products. It also suggests that the r_e, tau, and LWP of heavily precipitating clouds are biased low to an extent that is yet to be explored.

4.3. Sensor Resolution Issues

The retrieval of cloud properties assumes a homogeneously filled field of view and flat cloud tops. However, cloud inhomogeneity incurs partial pixel filling that leads to an underestimation of cloud optical depth and a respective overestimate of cloud drop effective radius (Z. Zhang et al., 2016). According to Equation 5, it can lead to either positive or negative biases in the retrieved N_d, depending on the inhomogeneity structure. Since the sub-pixel cloud structure is not resolved, the cloud fraction determination depends strongly on the threshold sensitivity to clouds within the pixel. Therefore, a higher resolution provides a more accurate cloud fraction. The cloud top temperature in convective clouds is averaged within the pixel. This leads to an underestimation of the cloud top temperature, maximum vertical extent, and LWP. While a better resolution decreases the biases due to partial pixel filling, it leads to greater biases due to the three-dimensional effects of cloud surfaces that are not horizontal. This problem is minimized when limiting the measurements to backscatter angles smaller than

30°, and using the more absorbing wavebands (e.g., 3.7 instead of 1.6 μm) for retrieving r_e and N_d (Rosenfeld et al., 2014).

4.4. Land Ocean Bias in Results/Published Estimates

Most satellite-based studies on ACI are limited to observations over the ocean. Estimates of the sensitivity of N_d to cloud-active aerosol over land are hampered by large retrieval uncertainties. The MODIS AOD product, which has been used for the majority of studies, is significantly less accurate over land than over the ocean. The uncertainty in MODIS retrievals of AOD was quantified at 0.03% + 0.05% over the ocean and 0.05% + 0.15% over the land by validating with AERONET (Levy et al., 2013; Remer et al., 2008). Additionally, the AOD retrievals over land have larger uncertainty over bright surfaces such as deserts and snow and often fail there (Hsu et al., 2006).

AE retrieval from MODIS over land is even more difficult leading to very poor retrieval capability (Levy et al., 2013), which limits the usefulness of the AI. Another reason for the differences between land and ocean is the existence of giant CCN originating from sea spray aerosols over the ocean, which partially counteract the susceptibility to fine aerosols (F. Liu et al., 2022; Pan et al., 2022). Cloud regimes are also different over land and ocean. For example, open cells uniquely occur over the ocean.

Gryspeerdt et al. (2017) have quantified global ERF_{aci} using MODIS AI data over both land and ocean. They note that their estimate over land is hampered by the limited quantitative skills of MODIS AI. As a result, they find very weak ERF_{aci} over land, and for some regions even a positive ERF_{aci}. For the same reason, Quaas et al. (2009) found a much smaller AOD-N_d susceptibility over land than over the ocean. McCoy et al. (2017) determined ERF_{aci} based on aerosol-cloud relationships based on SO_4 mass from MERRA reanalysis and N_d from MODIS. They selected cases based on the uniformity of the cloud cover, to get the most reliable N_d retrievals, which effectively means the majority of land regions were ignored. Jia et al. (2022) also used aerosol reanalysis data and restricted their analysis to ocean-only, because of the poor quality of the MODIS over-land aerosol data that were used in the reanalysis, and the difficulty in retrieving N_d over land regions from MODIS. Hasekamp et al. (2019b) used polarimetric PARASOL retrievals of (a proxy for) CCN columns together with MODIS N_d to quantify aerosol-N_d susceptibility and ERF_{aci} over the ocean. To translate the ERF_{aci} over the ocean to a global value of ERF_{aci}, they looked at the ratio $ERF_{aci\text{-}global}/ERF_{aci\text{-}ocean}$ in 13 different aerosol climate models. These models give a range of values for $RF_{aci\text{-}global}/RF_{aci\text{-}ocean}$ between 1.12 and 2.24, and a mean value of 1.5. When assuming that the global ocean susceptibility is also applicable over land, they would obtain an even larger value for the ratio of 1.64. The spread in the model values for this ratio is the largest contribution to the estimated uncertainty. Clearly, more accurate retrievals of both aerosol and cloud properties over land are needed to better quantify susceptibility and ERF_{aci}.

Additionally, the different aerosol types over the ocean and land have various effects on ACI. Fine aerosol (i.e., SO_4) nucleate more numerous and smaller cloud droplets as CCN (Twomey effect), suppressing warm rain by decreasing the collision–coalescence. This effect always enhances the cloud albedo and the resultant radiative cooling. In contrast, the giant cloud condensation nuclei (GCCN) that frequently occur as sea salt aerosol over the ocean can enhance the nucleation of fewer but larger cloud drops, accelerating warm rain initiation by larger initial cloud drop size (F. Liu et al., 2022; Rosenfeld et al., 2002; Yin et al., 2000). Numerous model studies supported that GCCN enhances warm rain production albeit with inconsistent magnitudes (Posselt et al., 2008; L'Ecuyer et al., 2009; Dror et al., 2020). The resulting fewer but larger cloud drops regulated by GCCN lead to expect a lower cloud albedo with the possible decrease LWP which is consumed by warm rain. However, recent observations show that added GCCN increases cloud drop effective radius and LWP (F. Liu et al., 2022).

Abundant coarse sea salt (CSS) particles released from sea spray are typical GCCN with high hygroscopicity (Chin et al., 2002; Randles et al., 2017). F. Liu et al. (2022) found that fine aerosols decreased rainfall flux and effective radius by a factor of 1/4% and 40% after fixing the CSS concentration and LWP, respectively. Conversely, for fixed fine aerosols and LWP, added CSS aerosols enhanced rainfall flux and r_e by a factor of 4% and 35%, respectively. These two-type aerosols show comparable but opposite effects on the marine warm clouds. Additionally, fine aerosols can invigorate and electrify deep clouds by suppressing warm rain (Koren et al., 2014; Pan et al., 2021; Rosenfeld et al., 2008). On the other hand, Pan et al. (2022) showed that CSS weakens the deep convection and resultant lightning through accelerating warm rain at the expense of mixed-phase precipitation. Added CSS can reduce the lightning by 90% when increasing CSS concentration from 10 to 100 μg cm^{-3},

explaining the large land-ocean contrasts in lightning. The opposite effects of fine aerosol and CSS on both shallow and deep marine clouds occur simultaneously and partially cancel each other. The combined effects of the two aerosol types should be considered for separating and quantifying the susceptibility and forcing due to anthropogenic emissions.

In summary of this section, cloud regimes can vary greatly with changing aerosols and other causes of self-organization under similar meteorological cloud controlling factors and over different surface types, notably land, and ocean. The variability of cloud regimes for given cloud-controlling factors with different aerosols constitutes the susceptibility of cloud properties to the aerosols. The susceptibilities should be separated into susceptibility to fine aerosols and to GCCN aerosols, where the coarse soluble aerosols prevail mostly over the ocean while anthropogenic emissions produce mostly fine aerosols with a hemispheric scale of long-range transport. In addition, sampling issues, particularly relating to data aggregation and the existence/accuracy of satellite retrievals must be considered when producing and comparing ERF_{aci} estimates. The bias toward ocean-only estimates in existing studies leaves a large uncertainty in the ERF_{aci} over land, demonstrated by the broad range in model estimates. With different cloud, meteorological and aerosol regimes found over land when compared to ocean, it is not clear that ocean-based studies can be translated into estimates of the ERF_{aci} over land.

5. Issues With N_d Susceptibility

The susceptibility of N_d to CCN is a well-known function of cloud base updraft and aerosol size distribution and composition. The challenge is retrieving the properties that determine the susceptibility at a global coverage by satellites. However, retrieving this susceptibility with satellite observations is subject to a number of issues that can introduce biases, which are addressed in this section.

5.1. Low Aerosol Conditions and the Aerosol Optical Signal

The reliance on the aerosol optical signal for satellite studies has the potential to bias estimates of the N_d susceptibility. Due to their larger cross-sectional area, large aerosol particles have a stronger scattering signal and so a larger contribution to the AOD and other optical properties (Horvath, 2014). While the particles with diameters >∼100 nm are the most important for the CCN concentration (Dusek et al., 2006), a lack of sensitivity of the optical signal to smaller particles may lead to a bias in the sensitivity in situations where small (or ultrafine) particles are nucleated to cloud droplets (J. Fan et al., 2018; P. L. Ma et al., 2018; X. Ma et al., 2018).

Accurate retrieval of the aerosol signal requires it to be separated from atmospheric and surface signals. When the aerosol signal is small, the uncertainty in the surface properties dominates the overall retrieval uncertainty, leading to large relative uncertainties in the aerosol signal. Furthermore, since aerosol effects on clouds are relative to the fractional change in aerosols, small non-discernible changes in absolute aerosol amounts in very clean situations can be large fractional changes that can lead to correspondingly large differences in cloud properties. This uncertainty in the aerosol signal and hence CCN in low aerosol (clean) conditions drives the diversity of observational estimates of the N_d susceptibility to aerosol, as well as providing a significant source of variation in GCM estimates of the ERF_{aci} (Gryspeerdt et al., 2023).

Since clouds are aerosol limited in low aerosol conditions, the usage of the retrieved CCN based on retrieved N_d and W_b (Section 3.4) may have advantages, as it would be the most accurate in these conditions, while optically based retrievals perform worst under these conditions.

5.2. The Dependence of Susceptibility on Updraft

N_d at the cloud base is a function of the aerosol number and vertical velocity. Thus, the cloud base updraft speed is expected to be the most relevant dynamical constraint among all cloud controlling factors as discussed in Section 2.2, as long as the updraft observations are possible.

The strong dependence of N_d susceptibility on updraft—producing larger susceptibility at stronger updraft—has been demonstrated by both observations and modeling, including in situ aircraft measurements (Berg et al., 2011; Jia, Ma, Yu, et al., 2019), ground-based remote sensing (McComiskey et al., 2009; Schmidt et al., 2015), and detailed parcel model simulations (Reutter et al., 2009). In practical terms, it is difficult to make direct observations of vertical velocity near the cloud base at a global scale, but it can be linked to CBH and cloud top radiative cooling rate (Zheng, 2019; Zheng et al., 2015, 2016). For example, a good linear correlation between CBH and

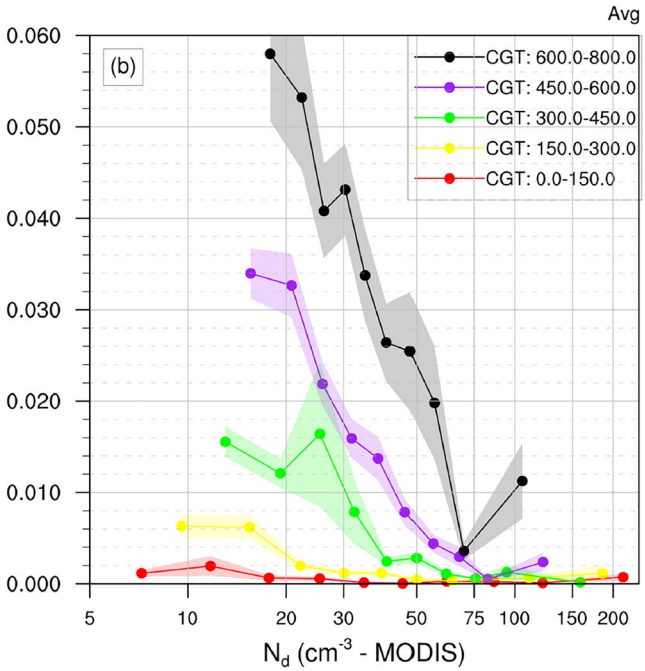

Figure 10. Average rain rate (mm/hr) from the Global Precipitation Mission radar as a function of Moderate Resolution Imaging Spectrometer-retrieved N_d and several cloud geometric thickness intervals. The data are for warm marine boundary layer clouds. From C. Fan et al. (2020).

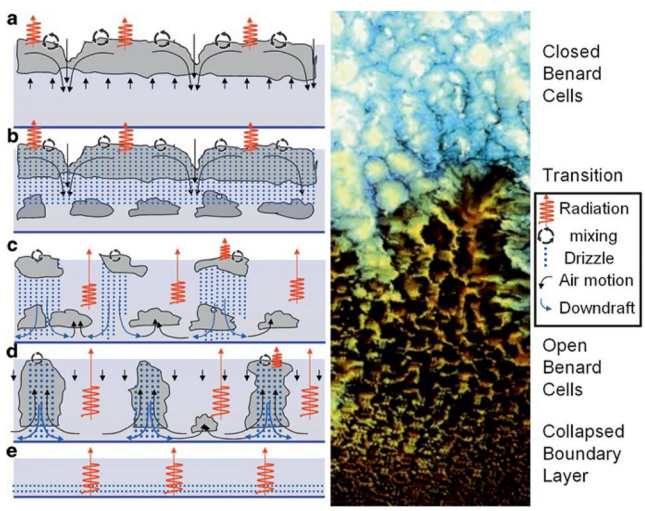

Figure 11. A schematic illustration of the mechanism for transition from non-precipitating closed cells of marine stratocumulus to precipitating open cells. Aerosol cloud processing in marine stratocumulus that are maintained by cloud-top radiative cooling (a) decreases aerosol and drop concentrations which initiate drizzle (b). The drizzle further scavenges aerosols that lead to enhanced coalescence and rain with downdrafts due to precipitation evaporative cooling (c). The downdrafts lead to the dissipation of their originating clouds and trigger new clouds, thereby breaking up the cloud cover (d). The positive feedback loop of precipitation-scavenging can lead in extreme cases to ultra-clean air where there have insufficient cloud drop condensation nuclei concentrations for sustaining cloud formation (e), as shown in Figure 1. After Rosenfeld et al. (2006).

vertical velocity at the base of a liquid cloud was observed by in situ observations, with stronger updrafts for higher CBH (Zheng et al., 2015). Thus, CBH directly retrieved from both active (Mülmenstädt et al., 2018) and passive remote sensing (Böhm et al., 2019) and cloud-top radiative cooling inferred from reanalysis data (Rosenfeld et al., 2019) could be promising proxies of updraft at a global scale. Additionally, the pixel-level CBH retrievals are more tightly linked to cloud-scale dynamics compared to large-scale meteorological condition constraints. Based on this strategy, Jia et al. (2022) found that N_d susceptibility to AOD (AI) increases linearly with CBH. A similar dependency on CGT was also seen but with a strong reduction in susceptibility when CGT was larger than 800 m (Jia et al., 2022). The susceptibility-updraft relationship could be promising in application to the estimation of global aerosol-cloud radiative forcing, by which the change in N_d from the PI to the PD can be inferred based on the climatology of updraft proxies from satellite and reanalysis products and anthropogenic aerosol emission perturbation assuming first-order unchanged distributions of updraft-proxies.

5.3. Precipitating State

Precipitation is a key confounding factor that influences both the aerosol and N_d, obscuring meaningful interpretations of the aerosol-N_d relation. Specifically, precipitation can modify the below cloud aerosol (that cannot be observed by satellites) via the wet scavenging effect (Gryspeerdt et al., 2015; Wood, 2006) and also co-varies with the near cloud aerosol via large-scale relative humidity (Boucher & Quaas, 2013; Grandey et al., 2014). Meanwhile, the coalescence and scavenging by precipitation act to reduce N_d as shown in Figure 10 (C. Fan et al., 2020; Jia et al., 2022) by the mechanism shown by Rosenfeld et al. (2006) (see Figure 11). As a result, a lower N_d sensitivity to AI has been observed for raining clouds than non–raining ones (Y.-C. Chen et al., 2014).

Cleaner air leads to larger and fewer cloud droplets with faster collisions and coalescence, leading to more rain that scavenges more aerosols and cleans the air further, leading to even more coalescence, rain, and scavenging in a positive feedback loop (Jing & Suzuki, 2018). This process widens the contrast between raining and non-raining clouds, as appears in the sharp borders between open and closed MCC, which is evident in Figure 8 and focused on in Figure 11. An outcome is a very large indicated susceptibility of cloud fraction and albedo to $N_{d,}$ which inherently includes both the primary aerosol effect and the precipitation scavenging feedback.

Quantifying the susceptibility to the raining and non-raining cloud scenes separately does not include the contribution of this positive feedback to the susceptibility. This partly explains why the largest indicated N_d sensitivity was obtained when considering all clouds together (Jia et al., 2022). Considering non-precipitating clouds solely is relevant to the activation term only without the feedback caused by precipitation scavenging of aerosol. Any inclusion of precipitation makes it difficult to correctly detect aerosol that actually interacts with the cloud with activation mechanism only, in turn, biasing the sensitivity to the cloud activation mechanism. This effect of aerosol–precipitation interaction and aerosol scavenging was reported to yield 21% larger N_d susceptibility compared to that for non-precipitating clouds that represents activation term only (Jia et al., 2022). Oddly, a positive sensitivity of the effective droplet radius to PM2.5 was found to dominate over China and became the physically expected negative sensitivity more frequently in the all-clouds case than in the non-raining case (Yang et al., 2021).

Furthermore, given that a sharp separation between precipitating and non-precipitating clouds does not exist in nature and is even harder to retrieve from passive satellites, most existing estimates of N_d sensitivity do not consider the influence of precipitation, or distinguish it roughly by relying on some simplified metrics, such as the threshold of $r_e = 14$ μm for rain initiation (Rosenfeld et al., 2019; J. Zhang et al., 2022) or the difference of CER between 2.1 and 3.7 μm bands (Jia, Ma, Quaas, et al., 2019; Saponaro et al., 2017). Active remote sensing can be used to explicitly distinguish precipitation, except in very shallow and low clouds. It should be noted that aerosol cloud processing also depletes the aerosols but to a lesser extent than precipitation. Therefore, in practice, it is very difficult not to incorporate aerosol scavenging feedback in the susceptibility.

Although this complicates the comparison between models and observations, the impact can be mitigated if the susceptibility calculated from the model is subject to the same precipitation-driven feedback processes.

5.4. Satellite Retrieval Biases of Aerosol and Cloud Properties

Fundamental assumptions for the N_d retrieval are 1D plane-parallel radiative transfer and overcast homogeneous cloud, that is, horizontal photon transport is ignored. This assumption works relatively well for clouds that are horizontally homogeneous at the satellite resolution scale (e.g., stratocumulus) but any retrievals made for broken, horizontally or vertically inhomogeneous clouds violate the assumptions, thereby appearing to overestimate r_e (Coakley et al., 2005), and in turn, underestimate N_d according to the Equation 5 (Quaas et al., 2006). Besides, aerosols above clouds can also bias the retrieval of cloud optical depth (Haywood et al., 2004; Li et al., 2014), in turn affecting N_d retrievals. It is important to not attribute such retrieval issues to ACI effects. These situations can be identified by lidar or reanalysis aerosol 3-dimensional distributions.

By evaluating satellite-derived N_d with in situ aircraft measurements (Gryspeerdt et al., 2022a), demonstrated that appropriate sampling strategies, such as focusing only on pixels with a high cloud fraction (Grosvenor et al., 2018) or a large cloud optical depth (Zhu et al., 2018), would help to sidestep the retrieval bias, though they have relatively little impact on the N_d sensitivity compared to the choice of CCN proxy. Meanwhile, when the aerosol properties are retrieved very close to the cloud by passive remote sensing, cloud contaminations (Kaufman et al., 2005) and cloud adjacency effect (Varnai and Marshak, 2009) play a role. Measuring the aerosol-indicated properties as a function of distance from the clouds, the biased AOD estimates (also applying to other CCN proxies) can be obtained. In most cases, the biases correspond to an overestimate in AOD but also underestimation may occur (Stap et al., 2016).

If the biases in N_d and CCN proxies co-vary with each other, a spurious correlation between the two variables is expected to occur, obscuring the causal interpretation of N_d susceptibility. A good example is the negative susceptibility found over land (Grandey & Stier, 2010, 2012; P. L. Ma et al., 2018; X. Ma et al., 2018) due to the poor retrieval capability (see Section 4.4). A negative susceptibility was even observed over the ocean when analyzing only partially cloudy pixels (Jia, Ma, Quaas, et al., 2019). Focusing on the retrievals over the ocean, Jia et al. (2022) suggested that retrieval biases of aerosol and cloud properties appear to underestimate the N_d susceptibility by ∼10%, in which CF in the retrieval grid-box is a key modulator. With increasing CF, the aerosol retrieval biases increase due to the enhanced near-cloud enhancement of AOD (AI), but cloud retrieval errors decrease due to the reduced cloud heterogeneity. This implies the difficulty in balancing the accuracies of both retrievals within the same grid in practical terms. In this regard, the use of aerosol reanalysis or retrieved CCN by N_d and W_b would be potential pathways to mitigate this issue.

5.5. Consistent Susceptibility and Anthropogenic Fraction

Although uncertainties in aerosol-cloud co-location can introduce biases in susceptibility estimates, they may not have a large impact on estimates of the RFaci and ERF_{aci}, as long as matching aerosol quantities are used for the susceptibility and the PI-PD difference (Gryspeerdt et al., 2017). This also applies when using different column aerosol products. However, a similar numerical susceptibility using AOD and SO_4 can lead to very different RFaci values, due to the different anthropogenic aerosol fractions for AOD and SO_4. Using retrieved CCN from N_d and W_b requires calculating the anthropogenic added CCN at relevant supersaturation with cloud-resolving models, which is presently a yet not fully resolved challenge. However, this will lead to susceptibilities that are closest to the physically based relationships between N_d and CCN, thus allowing to reduce uncertainties in models that use the actual physical processes. It should be noted that the biases in the susceptibility complicate comparisons to global models. This means that even in situations where the modeled susceptibility does not match

observations, the RF_{aci} could still be calculated accurately if a matching anthropogenic fraction was used. When using retrievals of N_d and cloud-base updraft for cloud-base CCN retrievals, it is necessary that the anthropogenic fraction of the CCN at the base of the specific clouds considered for the retrievals is simulated by models. This requires accurate simulations of CCN and sub-grid parameterization of the cloud base properties. This issue was discussed further in Section 4.1,

To summarize this section, quantifying the susceptibility of N_d to aerosols in a way that would be meaningful for use in GCM for calculating ERF_{aci} requires accounting for the following main considerations:

(a) The optical signal of the aerosols is biased toward the mass and not the number of concentrations. Losing the signal in the cleanest situations leads to a loss of sensitivity and underestimating the susceptibility.
(b) The susceptibility of N_d for the same aerosols depends on cloud-controlling factors, with cloud-base updraft being the most important one.
(c) The precipitation-scavenging positive feedback enhances the indicated susceptibility, but we cannot avoid it. Therefore, the GCMs should also include aerosol scavenging by precipitation for compatibility with observed susceptibilities when calculating ERF_{aci}.
(d) The retrieving of N_d and CCN proxies is plagued with biases that must be taken into account in calculating the uncertainty of the calculated susceptibility.
(e) The regimes for which the susceptibilities were defined and integrated with Equation 3 should match the observations and their definitions in GCMs for minimizing the bias in calculating of ERF_{aci}.

In summary, this section considered the difficulties in calculating the N_d susceptibility to aerosol, a critical term in Equation 3, of central importance to calculations of both the RFaci and ERF_{aci}. Uncertainties in both aerosol and cloud retrievals have a significant impact on susceptibility, particularly in clean and precipitating cases. The susceptibility also varies with regime, and with the aerosol proxy used to calculate it. These issues can be addressed by a careful regime-summation, as proposed in Equation 3, that takes into account these potentially bias-introducing factors. Care should also be taken to ensure that the anthropogenic aerosol fraction used matches the aerosol proxy used to calculate the susceptibility, both for ERF_{aci} estimates and for comparisons with GCMs.

6. Issues With Adjustment Terms

Cloud adjustments are the changes in clouds that occur in response to changes in aerosol. While N_d responds almost immediately to a change in aerosol, LWP and cloud fraction changes occur through a modification of precipitation and entrainment processes, requiring time to fully develop. Previous studies have indicated these adjustments could be large, but there are a number of issues with constraining them observationally.

6.1. Dealing With Non-Linearity

Non-linearity is particularly important when considering cloud fraction adjustments. While N_d and LWP are continuous fields, cloud cover has bounded between 0 and 1, and can be discontinuous. One of the important regimes where adjustments of cloud fraction to ACI occurs is stratocumulus (Sc). Sc transitions from closed to open cells occur when the clouds start precipitating strongly enough. This can occur in almost a step function, as illustrated in Figure 11. This roughly occurs when the cloud top effective radius reaches 15 μm, which is equivalent to N_d of about 50 cm^{-3} (Goren & Rosenfeld, 2014; Goren et al., 2019; Gryspeerdt et al., 2016; Rosenfeld et al., 2019). In that sense, aerosols affect non-linearly the Sc transitions, as more aerosols could not increase the Sc cloud fraction if they have already solid cloud cover. On the other hand, when considering the spatial-temporal evolution of the Sc at a large scale, the cloud fraction response to aerosols emerges as linear (Goren et al., 2019, 2022). This is so because closed cells with higher N_d need more time to produce strong enough precipitation. This time is equivalent to their spatial extent, assuming that the clouds are continuously advected. In other words, the higher the aerosol concentrations, the further fully cloudy closed cells are advected before breaking up into open cells (Goren et al., 2022). When considering the full domain of this occurrence, the cloud fraction increases more linearly with aerosols compared to what would expected from the small-scale behavior alone.

6.2. Feedbacks and Causality

The calculation of the adjustment terms depends on the covariation of different retrieved cloud properties. Even with perfect retrievals of cloud properties, the interconnected nature of the aerosol cloud system can lead to

positive feedbacks and to "buffering" (negative feedbacks) in the system obscuring the causal nature of links between the cloud properties (Stevens and Feingold, 2009). For example, if N_d leads to an increase in LWP, this could in turn lead to an increase in precipitation, reducing N_d (e.g., McCoy et al., 2020). Identifying the causal impact of N_d on LWP is difficult in this system due to these feedback processes. However, to the extent that the feedback occurs consistently with the primary effect, it could be considered a component of sensitivity. For example, the cloud fraction effect can be considered as an adjustment in response to the primary effect of aerosols on N_d, but the rain scavenging feedback can lead to large contrasts in cloud cover (see Figure 11) that may be responsible, according to some studies, for half of the ERF_{aci} or more (Bellouin et al., 2020; Rosenfeld et al., 2019). The inclusion of the feedback in the calculated susceptibility can still be used to constrain models if the GCM-calculated aerosols will include also the feedback processes that affect the aerosols, such as precipitation scavenging. Therefore, isolating the scavenging from the other effects by precipitating and nonprecipitating regimes would capture the practically inseparable processes of aerosol concentrations and their scavenging rates.

A controlled experiment can be used to uncover causal links in a system with this feedback. Natural experiments, where the aerosol is modified through some process independent of the local meteorology (e.g., shipping, volcanos) can be used as an effective tool to isolate causality. A variety of different natural experiments have been used to develop constraints on cloud adjustments, but they produce a diverse range of estimates (Christensen et al., 2022), may be limited by sampling biases (Glassmeier et al., 2021; Manshausen et al., 2022) and are not available under all conditions. Very large natural experiments, such as the Holohraun effusive volcanic eruption (Malavelle et al., 2017; McCoy & Hartmann, 2015) have a clearer link to climate-scale perturbations. However, with increasing scale comes a more complex definition of a control state, degrading the natural-experiment argument.

Temporal information can also be used to infer causality in an observed system (Pearl, 1994). Morning-afternoon variability using the pair of MODIS instruments has shown a link between aerosol and cloud evolution (Meskhidze et al., 2009). However, strong variability in the initial state can produce biases in the temporal development through regression-to-the-mean behavior (Gryspeerdt et al., 2022b) and it has proven difficult to use this behavior to develop strong constraints on the ERF_{aci}.

6.3. Retrieval Biases for Adjustments

The adjustment terms in Equation 3 depend strongly on the N_d. The retrieval issues of N_d are discussed in Section 5.5. Some biases, notably those depending on cloud adiabaticity and an accurate effective radius retrieval (Grosvenor et al., 2018) affect both N_d and other cloud properties or have magnitudes that are correlated to other cloud properties. Retrieval biases in the effective radius typically produce overestimates in r_e (depending on the near-IR wavelength used for the retrieval (Z. Zhang and Platnick, 2011); and hence underestimate N_d. These overestimates are typically larger in broken cloud regimes, leading to a relationship between N_d biases and CF, with a larger underestimate in N_d at low CF, biasing the adjustment terms. The bias due to broken clouds is overcome to a large extent by retrieving the N_d of only the cores of the clouds (Zhu et al., 2018). As both N_d and LWP retrievals rely on the r_e-retrieval, even random biases in r_e can produce spurious relationships between N_d and LWP, giving the appearance of an LWP adjustment (Arola et al., 2022). The use of an independent LWP retrieval (e.g., passive microwave) can reduce the magnitude of this bias (Gryspeerdt et al., 2019), but it may still have an important impact on observation-based assessments of the ERF_{aci}.

6.4. Cloud Fraction Definition

Cloud fraction of a given scene may vary with different observational methods. Linked to this variability are the LWP, cloud optical depth, and albedo. For example, a larger indicated cloud fraction due to the observational methodology would result in lower indicated LWP, cloud optical depth, and albedo.

Although the CF might be thought to be a simple parameter to measure, as it can be either cloudy or clear, this binary definition makes it challenging to define. Studies have shown that visible reflectance gradually decreases 10–20 km from the visible cloud edge (Eytan et al., 2020; Koren et al., 2007). They introduced this transitional zone as the clouds' twilight zone. This creates a challenge in setting the thresholds for the determination of a pixel being cloudy or clear (Platnick et al., 2003). These thresholds are often subjectively defined. The CF also strongly depends on the sensor's spatial resolution. For example, a high-resolution image with a spatial resolution of 250 m or less can show individual small-scale clouds and clouds boundaries, while a lower-resolution image

with a spatial resolution of 1 km or more may leave pixels with undetected small cloud features, or pixels that are only partially filled, to be classified as either cloudy or clear (G. Zhao and Di Girolamo, 2006). The time of observation (e.g., MODIS Aqua vs. Terra observations) can also affect the CF (Pincus et al., 1997), as observations later in the day tend to have lower CF over the ocean due to solar heating and cloud burning. The opposite occurs over land, where the CF can increase during the afternoon hours due to the diurnal heating that triggers convection. A large number of previous studies have shown strong evidence for a positive relationship between CF and N_d (Y.-C. Chen et al., 2014; Y. Chen et al., 2022; Goren & Rosenfeld, 2014; Goren et al., 2022; Gryspeerdt et al., 2016; Rosenfeld et al., 2019). However, the inconsistency among studies of the definition, resolution, and diurnal time of observation of CF, caused a large variability of the susceptibility of CF to N_d. This causes additional challenges when observations are used to constrain models, requiring the use of satellite simulators to produce meaningful comparisons.

6.5. Temperature Dependence

Both observational and model studies typically make the implicit assumption that the aerosol forcing is independent of the atmospheric state, particularly surface temperature. Cloud processes do not depend linearly on temperature, with changes in the cloud phase being the clearest example. This creates an implicit temperature dependence in the ERF_{aci} through changes in cloud phase (Mülmenstädt et al., 2021).

As many anthropogenic aerosols are poor ice-nucleating particles, a large modification of the ERF_{aci} from changes in cloud phase as a function of temperature is not expected. However, recent studies have shown that the LWP response to aerosol depends on lower tropospheric stability (the potential temperature difference between 700 and 1,000 hPa; Murray-Watson & Gryspeerdt, 2022; Zhou et al., 2021). Particularly in the Arctic, where surface temperatures are expected to increase faster than the free-troposphere, the expected decrease in stability leads to a weaker cooling from LWP adjustments in a future climate. These surface temperature dependencies for cloud adjustments and hence the ERF_{aci} should be accounted for when comparing observation-based and model ERF_{aci} estimates.

The main specific points of this section are summarized here:

(a) The magnitudes of the cloud fraction and LWP adjustments can be nonlinear with the magnitude of the perturbation.
(b) Much of the adjustments result from both negative and positive feedback processes which make it difficult to trace the cause and effect.
(c) Differential satellite retrieval biases to the adjusted cloud properties and the retrieved aerosol or N_d can distort the true relationships of the adjustment.
(d) As cloud fraction is a major adjusted cloud property, uncertainties in the determination of cloud fraction due to varying sensor resolution and cloud inhomogeneity distort respectively the inferred cloud fraction adjustment.
(e) The adjustment can vary with temperature and other cloud-controlling factors.

In summary, cloud adjustments to aerosols have large potential contributes to the ERF_{aci}, but there remain considerable challenges to accurately estimating their magnitude from observations. Satellite retrieval biases and feedbacks create difficulties in isolating the relationship between N_d and cloud properties. New statistical treatments and the use of natural experiments have led to progress in isolating causal relationships, but further development is still required. Non-linearities and temperature dependencies can create difficulties in extrapolating measurements of clouds in the present day to other climate states. This is an area of active research, but where possible, ERF_{aci} comparisons should be performed with the same background state.

7. Summary Recommendations and Outlook

7.1. New Retrievals and Missions

Polarimetric measurements with the National Aeronautics and Space Administration (NASA)'s planned Plankton, Aerosol, Cloud, ocean Ecosystem (PACE) mission are expected to provide improved accuracy for column-integrated aerosol properties from the SPEXone multi-angle polarimeter (Hasekamp et al., 2019b). Improvements in CCN (column) proxy are expected from higher accuracy in column number and size distribution as well as the possibility to quantify the aerosol water fraction and hence dry size distribution (Diedenhoven

et al., 2022). The Hyper-Angular Rainbow Polarimeter #2 (HARP-2) onboard PACE (McBride et al., 2020) can provide cloud r_e and ν_e (effective cloud droplet dispersion) retrievals that are virtually bias-free. Polarimetric retrievals of r_e and ν_e are typically representative of a vertical location in the cloud 50–100 m from the cloud top, while bi-spectral MODIS retrievals typically correspond to values deeper in the cloud. The spatial resolution of HARP-2 is 5 km which is coarser than MODIS.

For bi-spectral radiometric retrievals, increasing the satellite resolution greatly improves the accuracy of the retrievals of cloud optical depth, cloud fraction, r_e and N_d (Rosenfeld et al., 2014). Most of the scientific work has been based on the 1-km MODIS pixels. However, the MODIS is nearing its end of life and is being replaced by the VIIRS onboard the National Oceanic and Atmospheric Administration's new polar-orbiting satellites. The native resolution of the VIIRS is 750 m, and it has a subset Imager which is capable of retrieving cloud properties at a pixel resolution of 375 m (Rosenfeld et al., 2014). Using this high resolution made it possible to retrieve the T-r_e relationships in convective clouds and use them to retrieve $N_{d\text{-}ad}$, W_b and CCN (Rosenfeld et al., 2016). Unfortunately, the operational VIIRS cloud products are based only on the 750 m data, with no products for the 375 m data. However the increased resolution leads to a stronger impact of unresolved 3D effects on satellite retrievals, which will need to be better accounted for.

The METEOSAT Third Generation Flexible Combined Imager has visionary planning for ERF_{aci} applications. It has a nadir 500 m resolution at 0.64 and 2.2 μm, which allows the retrievals of warm clouds at 0.5 km resolution. It has 3.8 and 10.5 μm channels at a nadir resolution of 1 km with a full disk coverage every 10 min, which allows also the retrieval of cloud top temperature and phase at this spatial and temporal resolution, compared to the limitations of 2 km cloud products for the latest NOAA's Geostationary Operational Environmental Satellite. This should be very useful for documenting time-dependent processes and ascribing causality.

It is recommended to develop operational cloud products for the highest available resolution, because it will help overcome many of the cloud retrieval errors originating from partial footprint filling. It will also allow retrieving $N_{d\text{-}ad}$, which is presently possibly over land only with the VIIRS Imager with a resolution of 375 m (Rosenfeld et al., 2016). It is also recommended to design future operational satellites with spatial resolution of at least 1/3 km, although presently it failed to be recognized as a priority. The usage of the Environmental Mapping and Analysis Program (EnMAP, https://www.enmap.org/mission/) and Hyperspectral Precursor and Application Mission (https://www.eoportal.org/satellite-missions/prisma-hyperspectral#performance-specifications) (30 m) satellite missions could lead to a better understanding of ACI and aerosol-mediated cloud forcing. Polarimetric observations at such high spatial resolution are also recommended.

7.2. Recommendations for Improved Retrievals and Effective Forcing Calculations

(a) *Reporting of the radiative susceptibility/forcing for components of the ERF_{aci}.* The difficulty of creating a consistent definition of cloud properties (particularly cloud fraction) between different instruments and global models means that reporting susceptibilities for these quantities should be avoided. The use of the top of the atmosphere fluxes reduces the impact of varying cloud property definitions (e.g., cloud fraction) in susceptibility values. By reporting only the change to the TOA flux, a consistent set of cloud property retrievals can be used internally for the estimate, but does not have to be consistent with other methods. If the fluxes are employed in the susceptibility directly, this calculation does not depend on resolving the internal cloud structure within the scene. This is equivalent to the use of the dependence of scene average albedo on the aerosol proxy, bypassing the uncertainties in the retrieved cloud properties (Sections 6.3 and 6.4).

(b) Decomposition to Twomey $\left(\overline{\partial R}/\partial \ln N_d|_{LWP,f}\right)$, LWP $\left(\overline{\partial LWP}/\partial \ln N_d\right)$ and cloud cover $\left(\overline{\partial f}/\partial \ln N_d\right)$ effects should be done in a way that is constrained by the total scene CRE $\left(\overline{\partial R}/\partial \ln N_d\right)$, as mentioned in (a). The decomposition is useful mainly for constraining models by observations and for improved process understanding (Sections 6.3 and 6.4).

(c) For the derivation of the sensitivities for the adjustments of LWP and cloud cover, it is necessary to retrieve N_d and LWP independently from satellite measurements and to overcome the current approach to compute both from retrieved r_e and COD (Section 6.3).

(d) Include accurate cloud and aerosol retrievals under clean conditions, where the aerosol optical signal becomes very small and the cloud drop effective radius may be larger than the limits of the operational

retrieval algorithm. This may use models with assimilation of satellite observations of aerosols, improved aerosol retrievals from satellite instruments with improved sensitivity, or may be achieved by using $N_{d\text{-}ad}$ as a proxy for CCN concentrations (Section 5.1).

(e) The susceptibility should be calculated and integrated over different meteorological regimes which determine the thermodynamic and dynamical cloud properties independent of aerosols. The definition of suitable regimes depends on the process being investigated, but the characteristics of a good regime definition are outlined in Section 2.

(f) The widest possible range of aerosols should be included in the calculation of the susceptibility, including precipitating and non-rainy conditions. Cloud properties are dramatically affected by precipitation. Aerosols are scavenged by precipitation, and to a lesser extent also by non-precipitating aerosol cloud processing. The present assessments of susceptibilities of cloud properties to aerosols include these scavenging feedback processes. Separating the precipitation feedback from the susceptibility is needed to better employ observations to constrain processes in atmospheric models (Sections 4.1, 4.2, and 5.3).

(g) The ERF_{aci} based on (f) should be calculated by multiplying the susceptibilities by the atmospheric model calculations of added anthropogenic aerosols at the cloud base level, which include precipitation scavenging and cloud processing (Section 6.2).

(h) If a reanalysis model can correctly simulate aerosol processes, it provides a powerful tool for augmenting observational data, particularly in regions where the measurements are poor or non-existent. This gives it some advantages over AOD alone, as long as the atmospheric models can produce realistic natural and anthropogenic aerosol fields (Section 3.3).

(i) The next potential improvement after (h) is calculating explicitly the susceptibility of CRE to cloud base CCN, by using satellite-retrieved CCN(S_b), where S_b is cloud base supersaturation, based on $N_{d\text{-}ad}$ and W_b (Section 3.4).

(j) The application of (i) to calculating ERF_{aci} is possible as models become available that calculate the natural and added anthropogenic CCN(S_b) at the scale of cloud clusters, for weather-forecast models that reproduce the cloud stochastic properties sufficiently to match the satellite observations. The ERF_{aci} based on retrieved cloud base CCN should be calculated by multiplying the susceptibilities by the GCM calculations of natural and added anthropogenic CCN(S_b), including the effects of precipitation scavenging and cloud processing. This requires the development and validation of such GCM capabilities (Section 3.4).

(k) Joint aerosol-cloud retrieval algorithms need to be developed; currently, these algorithms are designed and maintained by different remote sensing communities.

7.3. Outlook

The trend of improved quality of the aerosol and cloud properties observations is associated with increased indicated susceptibilities and the resultant forcing (e.g., Hasekamp et al., 2019b; Rosenfeld et al., 2019). It was already suggested that ERF_{aci} was biased low when using AOD (Gryspeerdt et al., 2017; Penner et al., 2011), due to the limited information AOD provides about aerosol size and type. The most advanced aerosol retrieval based on the polarimetric aerosol retrievals resulted in RF_{aci} of -1.14 W m^{-2}, while its upper bound of -0.84 W m^{-2} equals the most likely value in AR6 (Hasekamp et al., 2019b). Ultimately, the susceptibility of cloud properties to CCN(S_b) is the most faithful measurement. The susceptibility of CRE to CCN(S_b) (Rosenfeld et al., 2019) was larger than any previously reported. The large susceptibility could be partially ascribed to the co-variability of aerosols and cloud properties, but it cannot explain the trend of increased susceptibility with increased fidelity of the retrievals. These larger RFaci estimates are closer to those produced by GCMs, but the current large uncertainty of model-based estimates highlights the need for improved constraints from observations. When combined with observational evidence of the behavior of liquid clouds, this stronger RFaci implies a considerably larger (more negative) ERF_{aci}. Such large negative forcing may challenge the top-down energy budget considerations (Murphy et al., 2009). Rosenfeld et al. (2019) suggested that a possible compensating mechanism may be positive radiative forcing by deep convective ice clouds, which have not yet been sufficiently quantified and constrained until now. While this review is limited to the problem of boundary layer water clouds, this possibility underlines the importance of investing comparable effort in deep and ice clouds.

Abbreviations

1D	One dimension
ACI	Aerosol-cloud interactions
AE	Angström exponent
AI	Aerosol index
ANR	Agence Nationale de la Recherche
AOD	Aerosol optical depth
AODf	Fine-mode aerosol optical depth
CALIOP	Cloud-aerosol lidar with orthogonal polarization
CALIPSO	Cloud-aerosol lidar and infrared pathfinder satellite observation
CBH	Cloud base height
CBT	Cloud base temperature
CCN	Cloud condensation nuclei
CF	Cloud fraction
CGT	Cloud geometrical thickness
COT	Cloud optical thickness
CRE	Cloud radiative effect
CSS	Coarse sea salt
CTH	Cloud top height
DFG	Deutsche Forschungsgemeinschaft
DLR	Deutsches Zentrum für Luft- und Raumfahrt
EnMAP	Environmental Mapping and Analysis Program
ERF_{ACI}	Effective radiative forcing of aerosol cloud interactions
FCI	Flexible combined imager
GC	Global climate model
GCCN	Giant cloud condensation nuclei
HARP-2	Hyper-angular rainbow polarimeter
IR	Infra-Red
ISSI	International Space Science Institute
LUT	Look-up-table
LWC	Liquid water content
LWP	Liquid water path
MERRA	Modern Era Retrospective analysis for Research and Applications
METEOSAT	METEOrological SATellite
MISR	Multi-angle Imaging SpectroRadiometer
MODIS	MODerate resolution Imaging Spectroadiometer
NASA	National Aeronautics and Space Administration
NIR	Near Infra-Red
NSFC	National Natural Science Foundation of China
PACE	Plankton, Aerosol, Cloud, ocean Ecosystem
PD	Present-day
PI	Pre-industrial
POLDER	POLarization and Directionality of Earth Reflectance
PRISMA	PRecursore IperSpettrale della Missione Applicativa
PSD	Particle size distribution
RFaci	Radiative Forcing of aerosol cloud interactions
Sc	Stratocumulus
SNPP	Suomi National Polar-orbiting Partnership
SPEXone	Spectro-Polarimeter for Exploration
SSA	Single Scattering Albedo
UTC	Coordinated Universal Time
UV	Ultra-violet
VIIRS	Visible Infrared Imaging Radiometer Suite

Data Availability Statement

As a review article, there are no new data analyses and respectively no data archival.

Acknowledgments
This work has been supported by the International Space Science Institute (ISSI) Bern in the framework of the ISSI International Team project #435 under the topic "Are we doing the right satellite observations and analyses for quantifying cloud-mediated aerosol climate forcing?'' (https://www.issibern.ch/teams/aeroclimforce/). We acknowledge the support of other team members including M. Christensen, G. Feingold, R. Kahn, T. Nakajima, S. Platnick, K. Suzuki and D. Winker. Alexander Kokhanovsky acknowledges the support of the EnMAP science program under the Space Agency at DLR with resources from the German Federal Ministry of Economic Affairs and Climate Action (Grant 50EE1923). Johannes Quaas, Tom Goren and Odran Sourdeval acknowledge support by ANR (ANR-20-CE92-0008) and DFG (GZ QU 311/27-1); Odran Sourdeval acknowledges support by the Centre National d'Etudes Spatiales (CNES) through the Expecting Earth-Care, Learning from A-Train (EECLAT) project; Johannes Quaas and Hailing Jia further acknowledge support by NSFC and DFG (GZ QU 311/28-1). Edward Gryspeerdt was supported by a Royal Society University Research Fellowship (URF/R1/191602).

References

Ackerman, A. S., Kirkpatrick, M. P., Stevens, D. E., & Toon, O. B. (2004). The impact of humidity above stratiform clouds on indirect aerosol climate forcing. *Nature*, *432*(7020), 1014–1017. https://doi.org/10.1038/nature03174

Ackerman, A. S., Toon, O. B., Stevens, D. E., Heymsfield, A. J., & Ramanathan, V. (2000). Reduction of tropical cloudiness by soot, Livermore, CA (United States). https://doi.org/10.2172/792796

Albrecht, B. A. (1989). Aerosols, cloud microphysics, and fractional cloudiness. *Science*, *245*(4923), 1227–1230. https://doi.org/10.1126/science.245.4923.1227

Alexandrov, M. D., Cairns, B., Emde, C., Ackerman, A. S., & van Diedenhoven, B. (2012). Accuracy assessments of cloud droplet size retrievals from polarized reflectance measurements by the research scanning polarimeter. *Remote Sensing of Environment*, *125*, 92–111. https://doi.org/10.1016/j.rse.2012.07.012

Alexandrov, M. D., Cairns, B., & Mishchenko, M. I. (2012). Rainbow fourier transform. *Journal of Quantitative Spectroscopy and Radiative Transfer*, *113*(18), 2521–2535. https://doi.org/10.1016/j.jqsrt.2012.03.025

Anderson, T. L., Charlson, R. J., Schwartz, S. E., Knutti, R., Boucher, O., Rodhe, H., & Heintzenberg, J. (2003a). Climate forcing by aerosols—A hazy picture. *Science*, *300*(5622), 1103–1104. https://doi.org/10.1126/science.1084777

Anderson, T. L., Charlson, R. J., Winker, D. M., Ogren, J. A., & Holmén, K. (2003b). Mesoscale variations of tropospheric aerosols. *Journal of the Atmospheric Sciences*, *60*(1), 119–136. https://doi.org/10.1175/1520-0469(2003)060<0119:mvota>2.0.co;2

Andreae, M. O. (2009). Correlation between cloud condensation nuclei concentration and aerosol optical thickness in remote and polluted regions. *Atmospheric Chemistry and Physics*, *9*(2), 543–556. https://doi.org/10.5194/acp-9-543-2009

Arola, A., Lipponen, A., Kolmonen, P., Virtanen, T., Bellouin, N., Grosvenor, D., et al. (2022). Aerosol effects on clouds are concealed by natural cloud heterogeneity and satellite retrieval errors. *Nature Communications*, *13*(1), 7357. https://doi.org/10.1038/s41467-022-34948-5

Bellouin, N., Quaas, J., Gryspeerdt, E., Kinne, S., Stier, P., Watson-Parris, D., et al. (2020). Bounding global aerosol radiative forcing of climate change. *Reviews of Geophysics*, *58*(1), e2019RG000660. https://doi.org/10.1029/2019rg000660

Berg, L. K., Berkowitz, C. M., Barnard, J. C., Senum, G., & Springston, S. R. (2011). Observations of the first aerosol indirect effect in shallow cumuli. *Geophysical Research Letters*, *38*(3), L03809. https://doi.org/10.1029/2010gl046047

Böhm, C., Sourdeval, O., Mülmenstädt, J., Quaas, J., & Crewell, S. (2019). Cloud base height retrieval from multi-angle satellite data. *Atmospheric Measurement Techniques*, *12*(3), 1841–1860. https://doi.org/10.5194/amt-12-1841-2019

Bony, S., Schulz, H., Vial, J., & Stevens, B. (2020). Sugar, gravel, fish, and flowers: Dependence of mesoscale patterns of trade-wind clouds on environmental conditions. *Geophysical Research Letters*, *47*(7), e2019GL085988. https://doi.org/10.1029/2019gl085988

Boucher, O., & Quaas, J. (2013). Water vapour affects both rain and aerosol optical depth. *Nature Geoscience*, *6*(1), 4–5. https://doi.org/10.1038/ngeo1692

Boucher, O., Randall, D., Artaxo, P., Bretherton, C., Feingold, G., Forster, P., et al. (2013). Clouds and aerosols. In T. Stocker, D. Qin, G.-K. Plattner, M. Tignor, S. Allen, J. Boschung, et al. (Eds.), *Climate change 2013: The physical science basis. Contribution of working group I to the fifth assessment report of the intergovernmental panel on climate change, chapter 7* (pp. 571–658). Cambridge University Press.

Bréon, F. M., & Colzy, S. (2000). Global distribution of cloud droplet effective radius from POLDER polarization measurements. *Geophysical Research Letters*, *27*(24), 4065–4068. https://doi.org/10.1029/2000gl011691

Breon, F. M., & Doutriaux-Boucher, M. (2005). A comparison of cloud droplet radii measured from space. *IEEE Transactions on Geoscience and Remote Sensing*, *43*(8), 1796–1805. https://doi.org/10.1109/TGRS.2005.852838

Bretherton, C. S., Blossey, P. N., & Uchida, J. (2007). Cloud droplet sedimentation, entrainment efficiency, and subtropical stratocumulus albedo. *Geophysical Research Letters*, *34*(3), L03813. https://doi.org/10.1029/2006GL027648

Cantrell, W., & Heymsfield, A. (2005). Production of ice in tropospheric clouds: A review. *Bulletin of the American Meteorological Society*, *86*(6), 795–808. https://doi.org/10.1175/bams-86-6-795

Carslaw, K. S., Lee, L. A., Reddington, C. L., Pringle, K. J., Rap, A., Forster, P. M., et al. (2013). Large contribution of natural aerosols to uncertainty in indirect forcing. *Nature*, *503*(7474), 67–71. https://doi.org/10.1038/nature12674

Chen, T. C., Xue, L., Lebo, Z. J., Wang, H., Rasmussen, R. M., & Seinfeld, J. H. (2011). A comprehensive numerical study of aerosol-cloud-precipitation interactions in marine stratocumulus. *Atmospheric Chemistry and Physics*, *11*(18), 9749–9769. https://doi.org/10.5194/acp-11-9749-2011

Chen, Y., Haywood, J., Wang, Y., Malavelle, F., Jordan, G., Partridge, D., et al. (2022). Machine learning reveals climate forcing from aerosols is dominated by increased cloud cover. *Nature Geoscience*, *15*(8), 609–614. https://doi.org/10.1038/s41561-022-00991-6

Chen, Y.-C., Christensen, M. W., Stephens, G. L., & Seinfeld, J. H. (2014). Satellite-based estimate of global aerosol–cloud radiative forcing by marine warm clouds. *Nature Geoscience*, *7*(9), 643–646. https://doi.org/10.1038/ngeo2214

Chin, M., Ginoux, P., Kinne, S., Torres, O., Holben, B. N., Duncan, B. N., et al. (2002). Tropospheric aerosol optical thickness from the GOCART model and comparisons with satellite and Sun photometer measurements. *Journal of the Atmospheric Sciences*, *59*(3), 461–483. https://doi.org/10.1175/1520-0469(2002)059<0461:taotft>2.0.co;2

Cho, H. M., Zhang, Z., Meyer, K., Lebsock, M., Platnick, S., Ackerman, A. S., et al. (2015). Frequency and causes of failed MODIS cloud property retrievals for liquid phase clouds over global oceans. *Journal of Geophysical Research: Atmospheres*, *120*(9), 4132–4154. https://doi.org/10.1002/2015jd023161

Choudhury, G., & Tesche, M. (2022). Estimating cloud condensation nuclei concentrations from CALIPSO lidar measurements. *Atmospheric Measurement Techniques*, *15*(3), 639–654. https://doi.org/10.5194/amt-15-639-2022

Christensen, M., Gettelman, A., Cermak, J., Dagan, G., Diamond, M., Douglas, A., et al. (2022). Opportunistic experiments to constrain aerosol effective radiative forcing. *Atmospheric Chemistry and Physics*, *22*(1), 641–674. https://doi.org/10.5194/acp-22-641-2022

Coakley, J. A., Friedman, M. A., & Tahnk, W. R. (2005). Retrieval of cloud properties for partly cloudy imager pixels. *Journal of Atmospheric and Oceanic Technology*, *22*(1), 3–17. https://doi.org/10.1175/jtech-1681.1

Coopman, Q., Riedi, J., Finch, D. P., & Garrett, T. J. (2018). Evidence for changes in arctic cloud phase due to long-range pollution transport. *Geophysical Research Letters*, *45*(19), 10709–10718. https://doi.org/10.1029/2018GL079873

Dagan, G., Koren, I., Altaratz, O., & Lehahn, Y. (2018). Shallow convective cloud field lifetime as a key factor for evaluating aerosol effects. *iScience*, *10*, 192–202. https://doi.org/10.1016/J.ISCI.2018.11.032

Di Noia, A., Hasekamp, O. P., van Diedenhoven, B., & Zhang, Z. (2019). Retrieval of liquid water cloud properties from POLDER-3 measurements using a neural network ensemble approach. *Atmospheric Measurement Techniques*, *12*(3), 1697–1716. https://doi.org/10.5194/amt-12-1697-2019

Dipu, S., Schwarz, M., Ekman, A. M. L., Gryspeerdt, E., Goren, T., Sourdeval, O., et al. (2022). Exploring satellite-derived relationships between cloud droplet number concentration and liquid water path using a large-domain large-eddy simulation. *Tellus B: Chemical and Physical Meteorology*, *74*(1), 176. https://doi.org/10.16993/tellusb.27

Donner, L. J., O'Brien, T. A., Rieger, D., Vogel, B., & Cooke, W. F. (2016). Are atmospheric updrafts a key to unlocking climate forcing and sensitivity? *Atmospheric Chemistry and Physics*, *16*(20), 12983–12992. https://doi.org/10.5194/acp-16-12983-2016

Dror, T., Flores, J. M., Altaratz, O., Dagan, G., Levin, Z., Vardi, A., & Koren, I. (2020). Sensitivity of warm clouds to large particles in measured marine aerosol size distributions—A theoretical study. *Atmospheric Chemistry and Physics*, *20*(23), 15297–15306. https://doi.org/10.5194/acp-20-15297-2020

Dubovik, O., Fuertes, D., Litvinov, P., Lopatin, A., Lapyonok, T., Doubovik, I., et al. (2019a). GRASP algorithm: Concept and application to remote sensing observations. *Journal of Quantitative Spectroscopy and Radiative Transfer*.

Dubovik, O., Li, Z., Mishchenko, M. I., Tanré, D., Karol, Y., Bojkov, B., et al. (2019b). Polarimetric remote sensing of atmospheric aerosols: Instruments, methodologies, results, and perspectives. *Journal of Quantitative Spectroscopy and Radiative Transfer*, *224*, 474–511. https://doi.org/10.1016/j.jqsrt.2018.11.024

Dubovik, O., Herman, M., Holdak, A., Lapyonok, T., Tanré, D., Deuzé, J. L., et al. (2011). Statistically optimized inversion algorithm for enhanced retrieval of aerosol properties from spectral multi-angle polarimetric satellite observations. *Atmospheric Measurement Techniques*, *4*(5), 975–1018. https://doi.org/10.5194/amt-4-975-2011

Dubovik, O., Sinyuk, A., Lapyonok, T., Holben, B. N., Mishchenko, M., Yang, P., et al. (2006). Application of spheroid models to account for aerosol particle nonsphericity in remote sensing of desert dust. *Journal of Geophysical Research*, *111*(D11), D11208. https://doi.org/10.1029/2005jd006619

Dusek, U., Frank, G. P., Hildebrandt, L., Curtius, J., Schneider, J., Walter, S., et al. (2006). Size matters more than chemistry for cloud-nucleating ability of aerosol particles. *Science*, *312*(5778), 1375–1378. https://doi.org/10.1126/science.1125261

Efraim, A., Rosenfeld, D., Schmale, J., & Zhu, Y. (2020). Satellite retrieval of cloud condensation nuclei concentrations in marine stratocumulus by using clouds as CCN chambers. *Journal of Geophysical Research: Atmospheres*, *125*(16), e2020JD032409. https://doi.org/10.1029/2020JD032409

Eytan, E., Koren, I., Altaratz, O., Kostinski, A. B., & Ronen, A. (2020). Longwave radiative effect of the cloud twilight zone. *Nature Geoscience*, *13*(10), 669–673. https://doi.org/10.1038/s41561-020-0636-8

Fan, C., Wang, M., Rosenfeld, D., Zhu, Y., Liu, J., & Chen, B. (2020). Strong precipitation suppression by aerosols in marine low clouds. *Geophysical Research Letters*, *47*(7), e2019GL086207. https://doi.org/10.1029/2019GL086207

Fan, J., Leung, L. R., Rosenfeld, D., Chen, Q., Li, Z., Zhang, J., & Yan, H. (2013). Microphysical effects determine macrophysical response for aerosol impacts on deep convective clouds. *Proceedings of the National Academy of Sciences of the United States of America*, *110*(48), E4581–E4590. https://doi.org/10.1073/pnas.1316830110

Fan, J., Rosenfeld, D., Zhang, Y., Giangrande, S. E., Li, Z., Machado, L. A. T., et al. (2018). Substantial convection and precipitation enhancements by ultrafine aerosol particles. *Science*, *359*(6374), 411–418. https://doi.org/10.1126/science.aan8461

Fanourgakis, G. S., Kanakidou, M., Nenes, A., Bauer, S. E., Bergman, T., Carslaw, K. S., et al. (2019). Evaluation of global simulations of aerosol particle and cloud condensation nuclei number, with implications for cloud droplet formation. *Atmospheric Chemistry and Physics*, *19*(13), 8591–8617. https://doi.org/10.5194/acp-19-8591-2019

Feingold, G. (2003). Modeling of the first indirect effect: Analysis of measurement requirements. *Geophysical Research Letters*, *30*(19), 1997. https://doi.org/10.1029/2003gl017967

Feingold, G., Eberhard, W. L., Veron, D. E., & Previdi, M. (2003). First measurements of the Twomey indirect effect using ground-based remote sensors. *Geophysical Research Letters*, *30*(6), 1287. https://doi.org/10.1029/2002GL016633

Feingold, G., Goren, T., & Yamaguchi, T. (2022). Quantifying albedo susceptibility biases in shallow clouds. *Atmospheric Chemistry and Physics*, *22*(5), 3303–3319. https://doi.org/10.5194/acp-22-3303-2022

Forster, P., Storelvmo, T., Armour, K., Collins, W., Dufresne, J.-L., Frame, D., et al. (2021). The earth's energy budget, climate feedbacks, and climate sensitivity. In V. Masson-Delmotte, P. Zhai, A. Pirani, S. Connors, C. Péan, S. Berger, et al. (Eds.), *Climate change 2021: The physical science basis. Contribution of working group I to the sixth assessment report of the intergovernmental panel on climate change, chapter 7* (pp. 923–1054). Cambridge University Press.

Freud, E., & Rosenfeld, D. (2012). Linear relation between convective cloud drop number concentration and depth for rain initiation. *Journal of Geophysical Research*, *117*(2), D02207. https://doi.org/10.1029/2011JD016457

Fu, G., Hasekamp, O., Rietjens, J., Smit, M., Di Noia, A., Cairns, B., et al. (2020). Aerosol retrievals from different polarimeters during the ACEPOL campaign using a common retrieval algorithm. *Atmospheric Measurement Techniques*, *13*(2), 553–573. https://doi.org/10.5194/amt-13-553-2020

Gettelman, A., Morrison, H., Santos, S., Bogenschutz, P., & Caldwell, P. M. (2015). Advanced two-moment bulk microphysics for global models. Part II: Global model solutions and aerosol–cloud interactions. *Journal of Climate*, *28*(3), 1288–1307. https://doi.org/10.1175/jcli-d-14-00103.1

Glassmeier, F., Hoffmann, F., Johnson, J. S., Yamaguchi, T., Carslaw, K. S., & Feingold, G. (2021). Aerosol-cloud-climate cooling overestimated by ship-track data. *Science*, *371*(6528), 485–489. https://doi.org/10.1126/science.abd3980

Goren, T., Feingold, G., Gryspeerdt, E., Kazil, J., Kretzschmar, J., Jia, H., & Quaas, J. (2022). Projecting stratocumulus transitions on the albedo—Cloud fraction relationship reveals linearity of albedo to droplet concentrations. *Geophysical Research Letters*, *49*(20), e2022GL101169. https://doi.org/10.1029/2022gl101169

Goren, T., Kazil, J., Hoffmann, F., Yamaguchi, T., & Feingold, G. (2019). Anthropogenic air pollution delays marine stratocumulus breakup to open cells. *Geophysical Research Letters*, *46*(23), 14135–14144. https://doi.org/10.1029/2019gl085412

Goren, T., & Rosenfeld, D. (2014). Decomposing aerosol cloud radiative effects into cloud cover, liquid water path and Twomey components in marine stratocumulus. *Atmospheric Research*, *138*, 378–393. https://doi.org/10.1016/j.atmosres.2013.12.008

Goren, T., Rosenfeld, D., Sourdeval, O., & Quaas, J. (2018). Satellite observations of precipitating marine stratocumulus show greater cloud fraction for decoupled clouds in comparison to coupled clouds. *Geophysical Research Letters*, *45*(10), 5126–5134. https://doi.org/10.1029/2018gl078122

Grandey, B. S., Gururaj, A., Stier, P., & Wagner, T. M. (2014). Rainfall-aerosol relationships explained by wet scavenging and humidity. *Geophysical Research Letters*, *41*(15), 5678–5684. https://doi.org/10.1002/2014gl060958

Grandey, B. S., & Stier, P. (2010). A critical look at spatial scale choices in satellite-based aerosol indirect effect studies. *Atmospheric Chemistry and Physics*, *10*(23), 11459–11470. https://doi.org/10.5194/acp-10-11459-2010

Grosvenor, D. P., Sourdeval, O., Zuidema, P., Ackerman, A., Alexandrov, M. D., Bennartz, R., et al. (2018). Remote sensing of droplet number concentration in warm clouds: A review of the current state of knowledge and perspectives. *Reviews of Geophysics*, *56*(2), 409–453. https://doi.org/10.1029/2017rg000593

Gryspeerdt, E., Glassmeier, F., Feingold, G., Hoffmann, F., & Murray-Watson, R. J. (2022a). Observing short-timescale cloud development to constrain aerosol–cloud interactions. *Atmospheric Chemistry and Physics*, *22*(17), 11727–11738. https://doi.org/10.5194/acp-22-11727-2022

Gryspeerdt, E., Goren, T., Sourdeval, O., Quaas, J., Mülmenstädt, J., Dipu, S., et al. (2019). Constraining the aerosol influence on cloud liquid water path. *Atmospheric Chemistry and Physics*, *19*(8), 5331–5347. https://doi.org/10.5194/acp-19-5331-2019

Gryspeerdt, E., McCoy, D. T., Crosbie, E., Moore, R. H., Nott, G. J., Painemal, D., et al. (2022b). The impact of sampling strategy on the cloud droplet number concentration estimated from satellite data. *Atmospheric Measurement Techniques*, *15*(12), 3875–3892. https://doi.org/10.5194/amt-15-3875-2022

Gryspeerdt, E., Povey, A. C., Grainger, R. G., Hasekamp, O., Hsu, N. C., Mulcahy, J. P., et al. (2023). Uncertainty in aerosol–cloud radiative forcing is driven by clean conditions. *Atmospheric Chemistry and Physics*, *23*(7), 4115–4122. https://doi.org/10.5194/acp-23-4115-2023

Gryspeerdt, E., Quaas, J., & Bellouin, N. (2016). Constraining the aerosol influence on cloud fraction. *Journal of Geophysical Research*, *121*(7), 3566–3583. https://doi.org/10.1002/2015jd023744

Gryspeerdt, E., Quaas, J., Ferrachat, S., Gettelman, A., Ghan, S., Lohmann, U., et al. (2017). Constraining the instantaneous aerosol influence on cloud albedo. *Proceedings of the National Academy of Sciences*, *114*(19), 4899–4904. https://doi.org/10.1073/pnas.1617765114

Gryspeerdt, E., Sourdeval, O., Quaas, J., Delanoë, J., Krämer, M., & Kühne, P. (2018). Ice crystal number concentration estimates from lidar–radar satellite remote sensing—Part 2: Controls on the ice crystal number concentration. *Atmospheric Chemistry and Physics*, *18*(19), 14351–14370. https://doi.org/10.5194/acp-18-14351-2018

Gryspeerdt, E., & Stier, P. (2012). Regime-based analysis of aerosol-cloud interactions. *Geophysical Research Letters*, *39*(21), 21802. https://doi.org/10.1029/2012gl053221

Gryspeerdt, E., Stier, P., & Partridge, D. G. (2014). Satellite observations of cloud regime development: The role of aerosol processes. *Atmospheric Chemistry and Physics*, *14*(3), 1141–1158. https://doi.org/10.5194/acp-14-1141-2014

Gryspeerdt, E., Stier, P., White, B. A., & Kipling, Z. (2015). Wet scavenging limits the detection of aerosol effects on precipitation. *Atmospheric Chemistry and Physics*, *15*(13), 7557–7570. https://doi.org/10.5194/acp-15-7557-2015

Hasekamp, O. P., Fu, G., Rusli, S. P., Wu, L., Di Noia, A., Aan de Brugh, J., et al. (2019a). Aerosol measurements by SPEXone on the NASA PACE mission: Expected retrieval capabilities. *Journal of Quantitative Spectroscopy and Radiative Transfer*, *227*, 170–184. https://doi.org/10.1016/j.jqsrt.2019.02.006

Hasekamp, O. P., Gryspeerdt, E., & Quaas, J. (2019b). Analysis of polarimetric satellite measurements suggests stronger cooling due to aerosol-cloud interactions. *Nature Communications*, *27*, 5405. https://doi.org/10.1038/s41467-019-13372-2

Hasekamp, O. P., & Landgraf, J. (2007). Retrieval of aerosol properties over land surfaces: Capabilities of multiple-viewing-angle intensity and polarization measurements. *Applied Optics*, *46*(16), 3332–3344. https://doi.org/10.1364/AO.46.003332

Hasekamp, O. P., Litvinov, P., & Butz, A. (2011). Aerosol properties over the ocean from PARASOL multiangle photopolarimetric measurements. *Journal of Geophysical Research*, *116*(D14), D14204. https://doi.org/10.1029/2010JD015469

Haywood, J. M., Osborne, S. R., & Abel, S. J. (2004). The effect of overlying absorbing aerosol layers on remote sensing retrievals of cloud effective radius and cloud optical depth. *Quarterly Journal of the Royal Meteorological Society*, *130*(598), 779–800. https://doi.org/10.1256/qj.03.100

Hoose, C., & Möhler, O. (2012). Heterogeneous ice nucleation on atmospheric aerosols: A review of results from laboratory experiments. *Atmospheric Chemistry and Physics*, *12*(20), 9817–9854. https://doi.org/10.5194/acp-12-9817-2012

Horvath, H. (2014). Basic optics, aerosol optics, and the role of scattering for sky radiance. *Journal of Quantitative Spectroscopy and Radiative Transfer*, *139*, 3–12. https://doi.org/10.1016/j.jqsrt.2013.08.009

Howard, L. (1803). Essay on the modifications of clouds.

Hsu, N. C., Tsay, S. C., King, M. D., & Herman, J. R. (2006). Deep blue retrievals of Asian aerosol properties during ACE-Asia. *IEEE Transactions on Geoscience and Remote Sensing*, *44*(11), 3180–3195. https://doi.org/10.1109/tgrs.2006.879540

Hu, S., Zhu, Y., Rosenfeld, D., Mao, F., Lu, X., Pan, Z., et al. (2021). The dependence of ship-polluted marine cloud properties and radiative forcing on background drop concentrations. *Journal of Geophysical Research: Atmospheres*, *126*(7), e2020JD033852. https://doi.org/10.1029/2020jd033852

Hu, Y., Lu, X., Zhai, P.-W., Hostetler, C. A., Hair, J. W., Cairns, B., et al. (2021). Liquid phase cloud microphysical property estimates from CALIPSO measurements. *Frontiers in Remote Sensing*, *2*, 25. https://doi.org/10.3389/frsen.2021.724615

Hu, Y., Vaughan, M., McClain, C., Behrenfeld, M., Maring, H., Anderson, D., et al. (2007). Global statistics of liquid water content and effective number concentration of water clouds over ocean derived from combined CALIPSO and MODIS measurements. *Atmospheric Chemistry and Physics*, *7*(12), 3353–3359. https://doi.org/10.5194/acp-7-3353-2007

Inness, A., Ades, M., Agustí-Panareda, A., Barré, J., Benedictow, A., Blechschmidt, A.-M., et al. (2019). The CAMS reanalysis of atmospheric composition. *Atmospheric Chemistry and Physics*, *19*(6), 3515–3556. https://doi.org/10.5194/acp-19-3515-2019

Jakob, C., & Tselioudis, G. (2003). Objective identification of cloud regimes in the tropical western pacific. *Geophysical Research Letters*, *30*(21), 2082. https://doi.org/10.1029/2003gl018367

Jia, H., Ma, X., Quaas, J., Yin, Y., & Qiu, T. (2019). Is positive correlation between cloud droplet effective radius and aerosol optical depth over land due to retrieval artifacts or real physical processes? *Atmospheric Chemistry and Physics*, *19*(13), 8879–8896. https://doi.org/10.5194/acp-19-8879-2019

Jia, H., Ma, X., Yu, F., Liu, Y., & Yin, Y. (2019). Distinct impacts of increased aerosols on cloud droplet number concentration of stratus/stratocumulus and cumulus. *Geophysical Research Letters*, *46*(22), 13517–13525. https://doi.org/10.1029/2019gl085081

Jia, H., Ma, X., Yu, F., & Quaas, J. (2021). Significant underestimation of radiative forcing by aerosol–cloud interactions derived from satellite-based methods. *Nature Communications*, *12*(1), 3649. https://doi.org/10.1038/s41467-021-23888-1

Jia, H., Quaas, J., Gryspeerdt, E., B¨ohm, C., & Sourdeval, O. (2022). Addressing the difficulties in quantifying droplet number response to aerosol from satellite observations. *Atmospheric Chemistry and Physics*, *22*(11), 7353–7372. https://doi.org/10.5194/acp-22-7353-2022

Jin, D., Oreopoulos, L., & Lee, D. (2017). Simplified ISCCP cloud regimes for evaluating cloudiness in CMIP5 models. *Climate Dynamics*, *48*(1–2), 113–130. https://doi.org/10.1007/s00382-016-3107-6

Jing, X., & Suzuki, K. (2018). The impact of process-based warm rain constraints on the aerosol indirect effect. *Geophysical Research Letters*, *45*(19), 10–729. https://doi.org/10.1029/2018gl079956

Kapustin, V., Clarke, A. D., Shinozuka, Y., Howell, S., Brekhovskikh, V., Nakajima, T., & Higurashi, A. (2006). On the determination of a cloud condensation nuclei from satellite: Challenges and possibilities. *Journal of Geophysical Research*, *111*(D4), D04202. https://doi.org/10.1029/2004jd005527

Kaufman, Y. J., Koren, I., Remer, L. A., Rosenfeld, D., & Rudich, Y. (2005). The effect of smoke, dust, and pollution aerosol on shallow cloud development over the atlantic ocean. *P. Natl. Acad. Sci. USA*, *102*(32), 11207–11212. https://doi.org/10.1073/pnas.0505191102

Knobelspiesse, K., Cairns, B., Mishchenko, M., Chowdhary, J., Tsigaridis, K., van Diedenhoven, B., et al. (2012). Analysis of fine-mode aerosol retrieval capabilities by different passive remote sensing instrument designs. *Optics Express*, *20*(19), 21457–21484. https://doi.org/10.1364/oe.20.021457

Köhler, H. (1936). The nucleus in and the growth of hygroscopic droplets. *Transactions of the Faraday Society*, *32*(2), 1152–1161. https://doi.org/10.1039/tf9363201152

Kokhanovsky, A. A. (2006). *Cloud optics*. Springer.

Koren, I., Dagan, G., & Altaratz, O. (2014). From aerosol-limited to invigoration of warm convective clouds. *Science*, *344*(6188), 1143–1146. https://doi.org/10.1126/science.1252595

Koren, I., Kaufman, Y. J., Remer, L. A., & Martins, J. V. (2004). Measurement of the effect of amazon smoke on inhibition of cloud formation. *Science*, *303*(5662), 1342–1345. https://doi.org/10.1126/science.1089424

Koren, I., Kaufman, Y. J., Rosenfeld, D., Remer, L. A., & Rudich, Y. (2005). Aerosol invigoration and restructuring of Atlantic convective clouds. *Geophysical Research Letters*, *32*(14), 519. https://doi.org/10.1029/2005gl023187

Koren, I., Oreopoulos, L., Feingold, G., Remer, L., & Altaratz, O. (2008). How small is a small cloud? *Atmospheric Chemistry and Physics*, *8*(14), 3855–3864. https://doi.org/10.5194/acp-8-3855-2008

Koren, I., Remer, L. A., Kaufman, Y. J., Rudich, Y., & Martins, J. V. (2007). On the twilight zone between clouds and aerosols. *Geophysical Research Letters*, *34*(8), 330. https://doi.org/10.1029/2007gl029253

Langton, T., Stier, P., Watson-Parris, D., & Mulcahy, J. P. (2021). Decomposing effective radiative forcing due to aerosol cloud interactions by global cloud regimes. *Geophysical Research Letters*, *48*(18), e2021GL093833. https://doi.org/10.1029/2021gl093833

L'Ecuyer, T. S., Berg, W., Haynes, J., Lebsock, M., & Takemura, T. (2009). Global observations of aerosol impacts on precipitation occurrence in warm maritime clouds. *Journal of Geophysical Research*, *114*(D9), D09211. https://doi.org/10.1029/2008jd011273

Levy, R. C., Mattoo, S., Munchak, L. A., Remer, L. A., Sayer, A. M., Patadia, F., & Hsu, N. C. (2013). The Collection 6 MODIS aerosol products over land and ocean. *Atmospheric Measurement Techniques*, *6*(11), 2989–3034. https://doi.org/10.5194/amt-6-2989-2013

Li, Z., Zhao, F., Liu, J., Jiang, M., Zhao, C., & Cribb, M. (2014). Opposite effects of absorbing aerosols on the retrievals of cloud optical depth from spaceborne and ground-based measurements. *Journal of Geophysical Research: Atmospheres*, *119*(9), 5104–5114. https://doi.org/10.1002/2013jd021053

Liu, F., Mao, F., Rosenfeld, D., Pan, Z., Zang, L., Zhu, Y., et al. (2022). Opposing comparable large effects of fine aerosols and coarse sea spray on marine warm clouds. *Communications Earth & Environment*, *3*(1), 1–9. https://doi.org/10.1038/s43247-022-00562-y

Liu, J., & Li, Z. (2014). Estimation of cloud condensation nuclei concentration from aerosol optical quantities: Influential factors and uncertainties. *Atmospheric Chemistry and Physics*, *14*(1), 471–483. https://doi.org/10.5194/acp-14-471-2014

Liu, Z., Wang, M., Rosenfeld, D., Zhu, Y., Bai, H., Cao, Y., & Liang, Y. (2020). Evaluation of cloud and precipitation response to aerosols in WRF-Chem with satellite observations. *Journal of Geophysical Research: Atmospheres*, *125*(18), e2020JD033108. https://doi.org/10.1029/2020jd033108

Loeb, N. G., & Manalo-Smith, N. (2005). Top-of-atmosphere direct radiative effect of aerosols over global oceans from merged CERES and MODIS observations. *Journal of Climate*, *18*(17), 3506–3526. https://doi.org/10.1175/jcli3504.1

Lohmann, U. (2008). Global anthropogenic aerosol effects on convective clouds in ECHAM5-HAM. *Atmospheric Chemistry and Physics*, *8*(7), 2115–2131. https://doi.org/10.5194/acp-8-2115-2008

Lopatin, A., Dubovik, O., Chaikovsky, A., Goloub, P., Lapyonok, T., Tanré, D., & Litvinov, P. (2013). Enhancement of aerosol characterization using synergy of lidar and sun-photometer coincident observations: The GARRLiC algorithm. *Atmospheric Measurement Techniques*, *6*(8), 2065–2088. https://doi.org/10.5194/amt-6-2065-2013

Lopatin, A., Dubovik, O., Fuertes, D., Stenchikov, G., Lapyonok, T., Veselovskii, I., et al. (2021). Synergy processing of diverse ground-based remote sensing and in situ data using the GRASP algorithm: Applications to radiometer, lidar and radiosonde observations. *Atmospheric Measurement Techniques*, *14*(3), 2575–2614. https://doi.org/10.5194/amt-14-2575-2021

Lu, X., Mao, F., Rosenfeld, D., Zhu, Y., Pan, Z., & Gong, W. (2021). Satellite retrieval of cloud base height and geometric thickness of low-level cloud based on CALIPSO. *Atmospheric Chemistry and Physics*, *21*(15), 11979–12003. https://doi.org/10.5194/acp-21-11979-2021

Lu, Z., Liu, X., Zhang, Z., Zhao, C., Meyer, K., Rajapakshe, C., et al. (2018). Biomass smoke from southern Africa can significantly enhance the brightness of stratocumulus over the southeastern Atlantic Ocean. *Proceedings of the National Academy of Sciences*, *115*(12), 2924–2929. https://doi.org/10.1073/pnas.1713703115

Ma, P.-L., Rasch, P., Wang, M., Wang, H., Ghan, S., Easter, R., et al. (2015). How does increasing horizontal resolution in a global climate model improve the simulation of aerosol-cloud interactions? *Geophysical Research Letters*, *42*(12), 5058–5065. https://doi.org/10.1002/2015GL064183

Ma, P. L., Rasch, P. J., Chepfer, H., Winker, D. M., & Ghan, S. J. (2018). Observational constraint on cloud susceptibility weakened by aerosol retrieval limitations. *Nature Communications*, *9*(1), 2640. https://doi.org/10.1038/s41467-018-05028-4

Ma, X., Jia, H., Yu, F., & Quaas, J. (2018). Opposite aerosol index-cloud droplet effective radius correlations over major industrial regions and their adjacent oceans. *Geophysical Research Letters*, *45*(11), 5771–5778. https://doi.org/10.1029/2018gl077562

Malavelle, F. F., Haywood, J. M., Jones, A., Gettelman, A., Clarisse, L., Bauduin, S., et al. (2017). Strong constraints on aerosol–cloud interactions from volcanic eruptions. *Nature*, *546*(7659), 485–491. https://doi.org/10.1038/nature22974

Manshausen, P., Watson-Parris, D., Christensen, M. W., Jalkanen, J. P., & Stier, P. (2022). Invisible ship tracks show large cloud sensitivity to aerosol. *Nature*, *610*(7930), 101–106. https://doi.org/10.1038/s41586-022-05122-0

McBride, B. A., Martins, J. V., Barbosa, H. M., Birmingham, W., & Remer, L. A. (2020). Spatial distribution of cloud droplet size properties from Airborne Hyper-Angular Rainbow Polarimeter (AirHARP) measurements. *Atmospheric Measurement Techniques*, *13*(4), 1777–1796. https://doi.org/10.5194/amt-13-1777-2020

McComiskey, A., Feingold, G., Frisch, A. S., Turner, D. D., Miller, M. A., Chiu, J. C., et al. (2009). An assessment of aerosol-cloud interactions in marine Stratus clouds based on surface remote sensing. *Journal of Geophysical Research*, *114*(D9), D09203. https://doi.org/10.1029/2008jd011006

McCoy, D. T., Bender, F. A.-M., Mohrmann, J. K. C., Hartmann, D. L., Wood, R., & Grosvenor, D. P. (2017). The global aerosol-cloud first indirect effect estimated using MODIS, MERRA, and AeroCom. *Journal of Geophysical Research: Atmospheres*, *122*(3), 1779–1796. https://doi.org/10.1002/2016jd026141

McCoy, D. T., Field, P., Gordon, H., Elsaesser, G. S., & Grosvenor, D. P. (2020). Untangling causality in midlatitude aerosol-cloud adjustments. *Atmospheric Chemistry and Physics*, *20*(7), 4085–4103. https://doi.org/10.5194/acp-20-4085-2020

McCoy, D. T., & Hartmann, D. L. (2015). Observations of a substantial cloud-aerosol indirect effect during the 2014–2015 Bárðarbunga-Veiðivötn fissure eruption in Iceland. *Geophysical Research Letters*, *42*(23), 10-409. https://doi.org/10.1002/2015GL067070

Medeiros, B., & Stevens, B. (2011). Revealing differences in GCM representations of low clouds. *Climate Dynamics*, *36*(1–2), 385–399. https://doi.org/10.1007/s00382-009-0694-5

Meskhidze, N., Remer, L. A., Platnick, S., Negrón Juárez, R., Lichtenberger, A. M., & Aiyyer, A. R. (2009). Exploring the differences in cloud properties observed by the Terra and Aqua MODIS Sensors. *Atmospheric Chemistry and Physics*, *9*(10), 3461–3475. https://doi.org/10.5194/acp-9-3461-2009

Mishchenko, M. I., Videen, G., Babenko, V. A., Khlebtsov, N. G., & Wriedt, T. (2004). T-Matrix theory of electromagnetic scattering by particles and its applications: A comprehensive reference database. *Journal of Quantitative Spectroscopy and Radiative Transfer*, *88*(1–3), 357–406.

Mohrmann, J., Wood, R., Yuan, T., Song, H., Eastman, R., & Oreopoulos, L. (2021). Identifying meteorological influences on marine low-cloud mesoscale morphology using satellite classifications. *Atmospheric Chemistry and Physics*, *21*(12), 9629–9642. https://doi.org/10.5194/acp-21-9629-2021

Mülmenstädt, J., Salzmann, M., Kay, J. E., Zelinka, M. D., Ma, P.-L., Nam, C., et al. (2021). An underestimated negative cloud feedback from cloud lifetime changes. *Nature Climate Change*, *11*(6), 508–513. https://doi.org/10.1038/s41558-021-01038-1

Mülmenstädt, J., Sourdeval, O., Henderson, D. S., l'Ecuyer, T. S., Unglaub, C., Jungandreas, L., et al. (2018). Using CALIOP to estimate cloud-field base height and its uncertainty: The cloud base altitude spatial extrapolator (CBASE) algorithm and dataset. *Earth System Science Data*, *10*(4), 2279–2293. https://doi.org/10.5194/essd-10-2279-2018

Murphy, D. M., Solomon, S., Portmann, R. W., Rosenlof, K. H., Forster, P. M., & Wong, T. (2009). An observationally based energy balance for the earth since 1950. *Journal of Geophysical Research*, *114*(D17), D17107. https://doi.org/10.1029/2009jd012105

Murray-Watson, R. J., & Gryspeerdt, E. (2022). Stability-dependent increases in liquid water with droplet number in the arctic. *Atmospheric Chemistry and Physics*, *22*(9), 5743–5756. https://doi.org/10.5194/acp-22-5743-2022

Nakajima, T., Higurashi, A., Kawamoto, K., & Penner, J. E. (2001). A possible correlation between satellite-derived cloud and aerosol microphysical parameters. *Geophysical Research Letters*, *28*(7), 1171–1174. https://doi.org/10.1029/2000gl012186

Nakajima, T., & King, M. D. (1990). Determination of the optical thickness and effective particle radius of clouds from reflected solar radiation measurements. Part I: Theory. *Journal of the Atmospheric Sciences*, *47*(15), 1878–1893. https://doi.org/10.1175/1520-0469(1990)047<1878:dotota>2.0.co;2

Nam, C. C., & Quaas, J. (2013). Geographically versus dynamically defined boundary layer cloud regimes and their use to evaluate general circulation model cloud parameterizations. *Geophysical Research Letters*, *40*(18), 4951–4956. https://doi.org/10.1002/grl.50945

Oreopoulos, L., Cho, N., Lee, D., Kato, S., & Huffman, G. J. (2014). An examination of the nature of global MODIS cloud regimes. *Journal of Geophysical Research: Atmospheres*, *119*(13), 8362–8383. https://doi.org/10.1002/2013jd021409

Painemal, D., Chang, F.-L., Ferrare, R., Burton, S., Li, Z., Smith, W. L., Jr., et al. (2020). Reducing uncertainties in satellite estimates of aerosol–cloud interactions over the subtropical ocean by integrating vertically resolved aerosol observations. *Atmospheric Chemistry and Physics*, *20*(12), 7167–7177. https://doi.org/10.5194/acp-20-7167-2020

Pan, Z., Mao, F., Rosenfeld, D., Zhu, Y., Zang, L., Lu, X., et al. (2022). Coarse Sea spray inhibits lightning. *Nature Communications*, *13*(1), 4289. https://doi.org/10.1038/s41467-022-31714-5

Pan, Z., Rosenfeld, D., Zhu, Y., Mao, F., Gong, W., Zang, L., & Lu, X. (2021). Observational quantification of aerosol invigoration for deep convective cloud lifecycle properties based on geostationary satellite. *Journal of Geophysical Research: Atmospheres*, *126*(9), e2020JD034275. https://doi.org/10.1029/2020jd034275

Pearl, J. (1994). A probabilistic calculus of actions. In R. Lopez de Mantaras & D. Poole (Eds.), *Uncertainty in artificial intelligence 10* (pp. 454–462). Morgan Kaufmann.

Peng, Y., & Lohmann, U. (2003). Sensitivity study of the spectral dispersion of the cloud droplet size distribution on the indirect aerosol effect. *Geophysical Research Letters*, *30*(10), 14-1. https://doi.org/10.1029/2003gl017192

Penner, J. E., Xu, L., & Wang, M. (2011). Satellite methods underestimate indirect climate forcing by aerosols. *Proceedings of the National Academy of Sciences*, *108*(33), 13404–13408. https://doi.org/10.1073/pnas.1018526108

Penner, J. E., Zhou, C., Garnier, A., & Mitchell, D. L. (2018). Anthropogenic aerosol indirect effects in cirrus clouds. *Journal of Geophysical Research: Atmospheres*, *123*(20), 11652–11677. https://doi.org/10.1029/2018JD029204

Petters, M. D., & Kreidenweis, S. M. (2007). A single parameter representation of hygroscopic growth and cloud condensation nucleus activity. *Atmospheric Chemistry and Physics*, *7*(8), 1961–1971. https://doi.org/10.5194/acp-7-1961-2007

Pincus, R., Baker, M. B., & Bretherton, C. S. (1997). What controls stratocumulus radiative properties? Lagrangian observations of cloud evolution. *Journal of the Atmospheric Sciences*, *54*(17), 2215–2236. https://doi.org/10.1175/1520-0469(1997)054<2215:wcsrpl>2.0.co;2

Pinsky, M., Khain, A., Mazin, I., & Korolev, A. (2012). Analytical estimation of droplet concentration at cloud base. *Journal of Geophysical Research*, *117*(D18), D18211. https://doi.org/10.1029/2012jd017753

Platnick, S. (2000). Vertical photon transport in cloud remote sensing problems. *Journal of Geophysical Research*, *105*(D18), 22919–22935. https://doi.org/10.1029/2000jd900333

Platnick, S., King, M. D., Ackerman, S. A., Menzel, W. P., Baum, B. A., Riédi, J. C., & Frey, R. A. (2003). The MODIS cloud products: Algorithms and examples from Terra. *IEEE Transactions on Geoscience and Remote Sensing*, *41*(2), 459–473. https://doi.org/10.1109/tgrs.2002.808301

Posselt, R., & Lohmann, U. (2008). Influence of giant CCN on warm rain processes in the ECHAM5 GCM. *Atmospheric Chemistry and Physics*, *8*(14), 3769–3788. https://doi.org/10.5194/acp-8-3769-2008

Quaas, J., Boucher, O., Bellouin, N., & Kinne, S. (2008). Satellite-based estimate of the direct and indirect aerosol climate forcing. *Journal of Geophysical Research*, *113*(D5), D05204. https://doi.org/10.1029/2007JD008962

Quaas, J., Boucher, O., & Lohmann, U. (2006). Constraining the total aerosol indirect effect in the LMDZ and ECHAM4 GCMs using MODIS satellite data. *Atmospheric Chemistry and Physics*, *6*(4), 947–955. https://doi.org/10.5194/acp-6-947-2006

Quaas, J., & Gryspeerdt, E. (2022). Aerosol-cloud interactions in liquid clouds (pp. 489–544).

Quaas, J., Ming, Y., Menon, S., Takemura, T., Wang, M., Penner, J. E., et al. (2009). Aerosol indirect effects—General circulation model intercomparison and evaluation with satellite data. *Atmospheric Chemistry and Physics*, *9*(22), 8697–8717. https://doi.org/10.5194/acp-9-8697-2009

Randles, C. A., Da Silva, A. M., Buchard, V., Colarco, P. R., Darmenov, A., Govindaraju, R., et al. (2017). The MERRA-2 aerosol reanalysis, 1980 onward. Part I: System description and data assimilation evaluation. *Journal of Climate*, *30*(17), 6823–6850. https://doi.org/10.1175/jcli-d-16-0609.1

Remer, L. A., Kleidman, R. G., Levy, R. C., Kaufman, Y. J., Tanré, D., Mattoo, S., et al. (2008). Global aerosol climatology from the MODIS satellite sensors. *Journal of Geophysical Research*, *113*(D14), D14S07. https://doi.org/10.1029/2007jd009661

Reutter, P., Su, H., Trentmann, J., Simmel, M., Rose, D., Gunthe, S. S., et al. (2009). Aerosol- and updraft-limited regimes of cloud droplet formation: Influence of particle number, size and hygroscopicity on the activation of cloud condensation nuclei (CCN). *Atmospheric Chemistry and Physics*, *9*(18), 7067–7080. https://doi.org/10.5194/acp-9-7067-2009

Rosenfeld, D., & Feingold, G. (2003). Explanation of discrepancies among satellite observations of the aerosol indirect effects. *Geophysical Research Letters*, *30*(14), 1776. https://doi.org/10.1029/2003GL017684
Rosenfeld, D., Kaufman, Y. J., & Koren, I. (2006). Switching cloud cover and dynamical regimes from open to closed Benard cells in response to the suppression of precipitation by aerosols. *Atmospheric Chemistry and Physics*, *6*(9), 2503–2511. https://doi.org/10.5194/acp-6-2503-2006
Rosenfeld, D., Lahav, R., Khain, A., & Pinsky, M. (2002). The role of sea spray in cleansing air pollution over ocean via cloud processes. *Science*, *297*(5587), 1667–1670. https://doi.org/10.1126/science.1073869
Rosenfeld, D., Liu, G., Yu, X., Zhu, Y., Dai, J., Xu, X., & Yue, Z. (2014). High resolution (375 m) cloud microstructure as seen from the NPP/VIIRS Satellite imager. *Atmospheric Chemistry and Physics*, *14*(5), 2479–2496. https://doi.org/10.5194/acp-14-2479-2014
Rosenfeld, D., Lohmann, U., Raga, G. B., O'Dowd, C. D., Kulmala, M., Fuzzi, S., et al. (2008). Flood or drought: How do aerosols affect precipitation? *Science*, *321*(5894), 1309–1313. https://doi.org/10.1126/science.1160606
Rosenfeld, D., & Woodley, W. L. (2003). Closing the 50-year circle: From cloud seeding to space and back to climate change through precipitation physics. Chapter 6 of "Cloud Systems, Hurricanes, and the Tropical Rainfall Measuring Mission (TRMM)". In W.-K. Tao & R. Adler (Eds.), *Meteorological monographs 51* (Vol. 234, pp. 59–80). AMS.
Rosenfeld, D., Zheng, Y., Hashimshoni, E., Pöhlker, M. L., Jefferson, A., Pöhlker, C., et al. (2016). Satellite retrieval of cloud condensation nuclei concentrations by using clouds as CCN chambers. *Proceedings of the National Academy of Sciences*, *113*(21), 5828–5834. https://doi.org/10.1073/pnas.1514044113
Rosenfeld, D., Zhu, Y., Wang, M., Zheng, Y., Goren, T., & Yu, S. (2019). Aerosol-driven droplet concentrations dominate coverage and water of oceanic low-level clouds. *Science*, *363*(6427), eaav0566. https://doi.org/10.1126/science.aav0566
Rossow, W. B., Zhang, Y., & Wang, J. (2005). A statistical model of cloud vertical structure based on reconciling cloud layer amounts inferred from satellites and radiosonde humidity profiles. *Journal of Climate*, *18*(17), 3587–3605. https://doi.org/10.1175/jcli3479.1
Saide, P., Carmichael, G., Spak, S., Minnis, P., & Ayers, J. (2012). Improving aerosol distributions below clouds by assimilating satellite-retrieved cloud droplet number. *Proceedings of the National Academy of Sciences*, *109*(30), 11939–11943. https://doi.org/10.1073/pnas.1205877109
Saponaro, G., Kolmonen, P., Sogacheva, L., Rodriguez, E., Virtanen, T., & de Leeuw, G. (2017). Estimates of the aerosol indirect effect over the Baltic Sea region derived from 12 years of MODIS observations. *Atmospheric Chemistry and Physics*, *17*(4), 3133–3143. https://doi.org/10.5194/acp-17-3133-2017
Schmidt, J., Ansmann, A., Bu¨hl, J., & Wandinger, U. (2015). Strong aerosol–cloud interaction in altocumulus during updraft periods: Lidar observations over central Europe. *Atmospheric Chemistry and Physics*, *15*(18), 10687–10700. https://doi.org/10.5194/acp-15-10687-2015
Song, X., & Zhang, G. J. (2011). Microphysics parameterization for convective clouds in a global climate model: Description and single-column model tests. *Journal of Geophysical Research*, *116*(D2), D02201. https://doi.org/10.1029/2010jd014833
Sourdeval, O., Gryspeerdt, E., Krämer, M., Goren, T., Delanoë, J., Afchine, A., et al. (2018). Ice crystal number concentration estimates from lidar–radar satellite remote sensing—Part 1: Method and evaluation. *Atmospheric Chemistry and Physics*, *18*(19), 14327–14350. https://doi.org/10.5194/acp-18-14327-2018
Sourdeval, O., Labonnote, C.-L., Baran, A. J., & Brogniez, G. (2015). A methodology for simultaneous retrieval of ice and liquid water cloud properties. Part I: Information content and case study. *Quarterly Journal of the Royal Meteorological Society*, *141*(688), 870–882. https://doi.org/10.1002/qj.2405
Stap, F. A., Hasekamp, O. P., Emde, C., & Röckmann, T. (2016). Multiangle photopolarimetric aerosol retrievals in the vicinity of clouds: Synthetic study based on a large eddy simulation. *Journal of Geophysical Research: Atmospheres*, *121*(21), 12–914. https://doi.org/10.1002/2016jd024787
Stevens, B., Acquistapace, C., Hansen, A., Heinze, R., Klinger, C., Klocke, D., et al. (2020a). Large-eddy and storm resolving models for climate prediction—The added value for clouds and precipitation. *Journal of the Meteorological Society of Japan*, *98*(2), 395–435. https://doi.org/10.2151/jmsj.2020-021
Stevens, B., Bony, S., Brogniez, H., Hentgen, L., Hohenegger, C., Kiemle, C., et al. (2020b). Sugar, gravel, fish and flowers: Mesoscale cloud patterns in the trade winds. *Quarterly Journal of the Royal Meteorological Society*, *146*(726), 141–152. https://doi.org/10.1002/qj.3662
Stevens, B., & Feingold, G. (2009). Untangling aerosol effects on clouds and precipitation in a buffered system. *Nature*, *461*(7264), 607–613. https://doi.org/10.1038/nature08281
Stevens, B., Fiedler, S., Kinne, S., Peters, K., Rast, S., Müsse, J., et al. (2016). Simple plumes: A parameterization of anthropogenic aerosol optical properties and an associated Twomey effect for climate studies. *Geoscientific Model Development Discussions*, *10*, 433–452. https://doi.org/10.5194/gmd-2016-189
Stier, P. (2016). Limitations of passive remote sensing to constrain global cloud condensation nuclei. *Atmospheric Chemistry and Physics*, *16*(10), 6595–6607. https://doi.org/10.5194/acp-16-6595-2016
Toll, V., Christensen, M., Gassó, S., & Bellouin, N. (2017). Volcano and ship tracks indicate excessive aerosol-induced cloud water increases in a climate model. *Geophysical Research Letters*, *44*(24), 12-492. https://doi.org/10.1002/2017gl075280
Tsikerdekis, A., Schutgens, N. A. J., & Hasekamp, O. P. (2021). Assimilating aerosol optical properties related to size and absorption from POLDER/PARASOL with an ensemble data assimilation system. *Atmospheric Chemistry and Physics*, *21*(4), 2637–2674. https://doi.org/10.5194/acp-21-2637-2021
Tsikerdekis, A., Schutgens, N. A. J., Fu, G., & Hasekamp, O. P. (2022). Estimating aerosol emission from SPEXone on the NASA PACE mission using an ensemble Kalman smoother: Observing system simulation experiments (OSSEs). *Geoscientific Model Development*, *15*(8), 3253–3279. https://doi.org/10.5194/gmd-15-3253-2022
Twomey, S. (1959). The nuclei of natural cloud formation part II: The supersaturation in natural clouds and the variation of cloud droplet concentration. *Geofisica Pura e Applicata*, *43*(1), 243–249. https://doi.org/10.1007/bf01993560
Twomey, S. (1974). Pollution and the planetary albedo. *Atmospheric Environment*, *8*(12), 1251–1256. https://doi.org/10.1016/0004-6981(74)90004-3
Twomey, S. (1977). The influence of pollution on the shortwave albedo of clouds. *Journal of the Atmospheric Sciences*, *34*(7), 1149–1152. https://doi.org/10.1175/1520-0469(1977)034<1149:TIOPOT>2.0.CO;2
van Diedenhoven, B., Hasekamp, O. P., Cairns, B., Schuster, G. L., Stamnes, S., Shook, M., & Ziemba, L. (2022). Remote sensing of aerosol water fraction, dry size distribution and soluble fraction using multi-angle, multi-spectral polarimetry. *Atmospheric Measurement Techniques*, *15*(24), 7411–7434. https://doi.org/10.5194/amt-15-7411-2022
van Diedenhoven, B., Hasekamp, O. P., & Landgraf, J. (2006). Efficient vector radiative transfer calculations in vertically inhomogeneous cloudy atmospheres. *Applied Optics*, *45*(23), 5993–6006. https://doi.org/10.1364/ao.45.005993
Varnai, T., & Marshak, A. (2009). MODIS observations of enhanced clear sky reflectance near clouds. *Geophysical Research Letters*, *36*(6), L06807. https://doi.org/10.1029/2008gl037089
Wang, Y., Zhu, Y., Wang, M., Rosenfeld, D., Gao, Y., Yao, X., et al. (2021). Validation of satellite—Retrieved CCN based on a cruise campaign over the polluted Northwestern Pacific Ocean. *Atmospheric Research*, *260*, 105722. https://doi.org/10.1016/j.atmosres.2021.105722

Watson-Parris, D., Schutgens, N., Winker, D., Burton, S. P., Ferrare, R. A., & Stier, P. (2018). On the limits of CALIOP for constraining modeled free tropospheric aerosol. *Geophysical Research Letters*, *45*(17), 9260–9266. https://doi.org/10.1029/2018gl078195

Watson-Parris, D., & Smith, C. J. (2022). Large uncertainty in future warming due to aerosol forcing. *Nature Climate Change*, *12*(12), 1111–1113. https://doi.org/10.1038/s41558-022-01516-0

Wen, G., Marshak, A., Cahalan, R. F., Remer, L. A., & Kleidman, R. G. (2007). 3-D aerosol-cloud radiative interaction observed in collocated MODIS and ASTER images of cumulus cloud fields. *Journal of Geophysical Research*, *112*(D13), D13204. https://doi.org/10.1029/2006jd008267

Werdell, P. J., Behrenfeld, M. J., Bontempi, P. S., Boss, E., Cairns, B., Davis, G. T., et al. (2019). The Plankton, Aerosol, Cloud, ocean ecosystem mission: Status, science, advances. *Bulletin of the American Meteorological Society*, *100*(9), 1775–1794. https://doi.org/10.1175/bams-d-18-0056.1

Wilcox, E. M. (2010). Stratocumulus cloud thickening beneath layers of absorbing smoke aerosol. *Atmospheric Chemistry and Physics*, *10*(23), 11769–11777. https://doi.org/10.5194/acp-10-11769-2010

Winker, D. M., Vaughan, M. A., Omar, A., Hu, Y., Powell, K. A., Liu, Z., et al. (2009). Overview of the CALIPSO mission and CALIOP data processing algorithms. *Journal of Atmospheric and Oceanic Technology*, *26*(11), 2310–2323. https://doi.org/10.1175/2009JTECHA1281.1

WMO. (1975). International cloud atlas, volume I—Manual on the observation of clouds and other meteors.

WMO. (2017). International cloud atlas.

Wood, R. (2006). Rate of loss of cloud droplets by coalescence in warm clouds. *Journal of Geophysical Research*, *111*(D21), D21205. https://doi.org/10.1029/2006jd007553

Yang, Y., Zhao, C., Wang, Y., Zhao, X., Sun, W., Yang, J., et al. (2021). Multi-source data based investigation of aerosol-cloud interaction over the North China plain and North of the Yangtze plain. *Journal of Geophysical Research: Atmospheres*, *126*(19), e2021JD035609. https://doi.org/10.1029/2021jd035609

Yin, Y., Levin, Z., Reisin, T. G., & Tzivion, S. (2000). The effects of giant cloud condensation nuclei on the development of precipitation in convective clouds—A numerical study. *Atmospheric Research*, *53*(1–3), 91–116. https://doi.org/10.1016/s0169-8095(99)00046-0

Yue, Z., Rosenfeld, D., Liu, G., Dai, J., Yu, X., Zhu, Y., et al. (2019). Automated mapping of convective clouds (AMCC) thermodynamical, microphysical and CCN properties from SNPP/VIIRS satellite data. *Journal of Applied Meteorology and Climatology*, *58*(4), 887–902. https://doi.org/10.1175/JAMC-D-18-0144.1

Zhang, J., Reid, J. S., & Holben, B. N. (2005). An analysis of potential cloud artifacts in MODIS over ocean aerosol optical thickness products. *Geophysical Research Letters*, *32*(15), L15803. https://doi.org/10.1029/2005gl023254

Zhang, J., Zhou, X., Goren, T., & Feingold, G. (2022). Albedo susceptibility of northeastern pacific stratocumulus: The role of covarying meteorological conditions. *Atmospheric Chemistry and Physics*, *22*(2), 861–880. https://doi.org/10.5194/acp-22-861-2022

Zhang, Z., & Platnick, S. (2011). An assessment of differences between cloud effective particle radius retrievals for marine water clouds from three MODIS spectral bands. *Journal of Geophysical Research*, *116*(D20), 20215. https://doi.org/10.1029/2011JD016216

Zhang, Z., Werner, F., Cho, H. M., Wind, G., Platnick, S., Ackerman, A. S., et al. (2016). A framework based on 2-D Taylor expansion for quantifying the impacts of subpixel reflectance variance and covariance on cloud optical thickness and effective radius retrievals based on the bispectral method. *Journal of Geophysical Research: Atmospheres*, *121*(12), 7007–7025. https://doi.org/10.1002/2016JD024837

Zhao, B., Liou, K.-N., Gu, Y., Jiang, J. H., Li, Q., Fu, R., et al. (2018). Impact of aerosols on ice crystal size. *Atmospheric Chemistry and Physics*, *18*(2), 1065–1078. https://doi.org/10.5194/acp-18-1065-2018

Zhao, G., & Di Girolamo, L. (2006). Cloud fraction errors for trade wind cumuli from EOS-Terra instruments. *Geophysical Research Letters*, *33*(20), L20802. https://doi.org/10.1029/2006gl027088

Zheng, Y. (2019). Theoretical understanding of the linear relationship between convective updrafts and cloud-base height for shallow cumulus clouds. Part I: Maritime conditions. *Journal of the Atmospheric Sciences*, *76*(8), 2539–2558. https://doi.org/10.1175/jas-d-18-0323.1

Zheng, Y., Rosenfeld, D., & Li, Z. (2015). Satellite inference of thermals and cloud-base updraft speeds based on retrieved surface and cloud-base temperatures. *Journal of the Atmospheric Sciences*, *72*(6), 2411–2428. https://doi.org/10.1175/JAS-D-14-0283.1

Zheng, Y., Rosenfeld, D., & Li, Z. (2016). Quantifying cloud base updraft speeds of marine stratocumulus from cloud top radiative cooling. *Geophysical Research Letters*, *43*(21), 11407–11413. https://doi.org/10.1002/2016gl071185

Zhou, X., Zhang, J., & Feingold, G. (2021). On the importance of sea surface temperature for aerosol-induced brightening of marine clouds and implications for cloud feedback in a future warmer climate. *Geophysical Research Letters*, *48*(24), e2021GL095896. https://doi.org/10.1029/2021gl095896

Zhu, J., & Penner, J. E. (2020). Radiative forcing of anthropogenic aerosols on cirrus clouds using a hybrid ice nucleation scheme. *Atmospheric Chemistry and Physics*, *20*(13), 7801–7827. https://doi.org/10.5194/acp-20-7801-2020

Zhu, Y., Rosenfeld, D., & Li, Z. (2018). Under what conditions can we trust retrieved cloud drop concentrations in broken marine stratocumulus? *Journal of Geophysical Research: Atmospheres*, *123*(16), 8754–8767. https://doi.org/10.1029/2017jd028083

Zhu, Y., Rosenfeld, D., Yu, X., Liu, G., Dai, J., & Xu, X. (2014). Satellite retrieval of convective cloud base temperature based on the NPP/VIIRS Imager. *Geophysical Research Letters*, *41*(4), 1308–1313. https://doi.org/10.1002/2013GL058970